LAPPEENRANTA UNIVERSITY OF TECHNOLOGY
School of Engineering Science
Laboratory of Green Chemistry
Chemical Engineering for Water Treatment

Olga Maliuk

SYNTHESIS AND APPLICATION OF LIGNIN-BASED ADSORBENTS FOR METAL CATIONS REMOVAL FROM WATER SOLUTIONS

Examiners: Prof. Mika Sillanpää
D.Sc. (Tech) Eveliina Repo

Instructor: M.Sc. (Tech) Nikolai Ponomarev

ABSTRACT

Lappeenranta University of Technology
School of Engineering Science
Laboratory of Green Chemistry
Chemical Engineering for Water Treatment

Olga Maliuk

Synthesis and application of lignin-based adsorbents for metal cations removal from water solutions

Master Thesis

2017

69 pages, 26 figures, 14 tables, and 5 appendices

Examiners: Prof. Mika Sillanpää
D. Sc. (Tech) Eveliina Repo
Instructor: M.Sc. (Tech) Nikolai Ponomarev

Keywords: lignin, magnesium hydroxide (brucite), nanocomposite, adsorption, heavy metals ions.

This research is focused on the development of a novel inexpensive and environmentally friendly nanocomposite materials that will act as adsorbents for the removal of Ni(II), Cd(II) and Pb(II) from aqueous solutions. In support of the trend of the sustainable use and minimization of industrial wastes, lignin was chosen as a biopolymer matrix for the nanocomposite synthesis. Brucite was incorporated into biopolymer matrix as a reinforcing material via co-precipitation method. One part of synthesized nanocomposite material was converted into a coal form by pyrolysis. Both obtained materials were investigated via different analytical methods. The affiliation of the synthesized materials with nanocomposites was confirmed by TEM and XRD. Presence of functional groups was detected by FTIR. The textural properties were examined via BET method. Thermal properties of the synthesized nanocomposites were determined by TGA and DTA. Adsorption properties of novel sorbents were studied as a function of dose, pH, temperature, contact time, and initial concentrations. In addition, the impact of competitive ions and multicomponent system were estimated and regeneration study carried out. Obtained experimental data were well correlated with the basic kinetics and isotherm models.

ACKNOWLEDGEMENTS

This research project would not have been possible without the opportunity to work in the Laboratory of Green Chemistry in Mikkeli, provided by Professor Mika Sillanpää and D. Sc. Eveliina Repo. I am grateful to The Regional Council of South-Savo for the financial support. I say “Thank you very much” to Nikolai Ponomarev for invaluable experience and skills that he gave me every day during my work in the laboratory. I highly appreciate Evgenia Iakovleva, Varsha Srivastava and Bhairavi Doshi for organization of analytical studies for my work. I am also thankful to all researchers of LGC for favorable working environment.

My profound gratitude goes to Alexander and my parents Konstantin and Galina for help and support on my way.

Mikkeli, November, 2017
Olga Maliuk

TABLE OF CONTENTS

LIST OF SYMBOLS

C_e – Equilibrium concentrations, (mmol/L; mg/L)

C_i – Initial concentration, (mmol/L)

m – Mass, (g)

V – Volume of the solution, (mL)

q_e – Equilibrium (maximum) adsorption, (mg/g; mmol/g);

q_t – Amount of adsorption at time (mg/g)

k_1 – First-order rate constant (min^{-1})

k_2 – Second-order rate constant (g/mg min)

$Q_{e.exp}$ – Experimental adsorption capacity (mg/g)

$Q_{e.theor}$ – Theoretically calculated adsorption capacity (mg/g)

t – Time (min)

C_0 – Concentration of an adsorbate at initial time (mg/L)

C_t – Concentration of an adsorbate at any time t (mg/L)

m_s – Dosage of an adsorbent in the solution (g/L)

q_m - Maximum adsorption capacity of adsorbent, (mg/g)

K_L- Energy of the adsorption, (L/mg)

K_F - Freundlich adsorption isotherm constant

n_F - Freundlich adsorption isotherm constant

n – Positive constant

LIST OF ABBREVIATIONS

BET – Brunauer, Emmet and Teller method

DI water – Double deionized water

DTA – Differential Thermal Analyses

ERRSQ – Sum of the square of the errors

EPA – Environmental Protection Agency

Eq – Equation

FTIR – Fourier Transform Infrared Spectroscopy

GAC – Granulated Activated Carbon

ICSD – Inorganic Crystal Structures Database

ICP-OES - Inductively Coupled Plasma Optical Emission Spectrometry

LH – Hydrolysis Lignin

MCL – Maximum Contaminated Level

MH – Magnesium Hydroxide

ppm – Measure of small concentrations – parts per million (10^{-6})

SSA - Specific Surface Area

TEM – Transmission Electron Microscopy

TGA – Thermal Gravimetrical Analysis

QS – Quality Sample

WWT – Waste Water Treatment

XRD – X-Ray Powder Diffraction

INTRODUCTION

The question of treating industrial wastewater containing heavy metal ions looms large nowadays. Because of anthropogenic activity, an overstock amount of contaminated water discharges into water bodies. Metal ions due to high solubility are able to be accumulated by living organisms and then embed into a food chain. Metal ions being hazardous elements at high concentrations adversely effect on organisms and the environment.

There are a lot of different definitions of the term "heavy metal" (Duffus, 2002). However, it is widely viewed that heavy metals are counted as metals with density at least 5 g/m^3 (Barakat, 2011). The target metal ions of present research that are needed to be removed from water are nickel, cadmium, and lead. They also belong to the group of heavy metals. As these metals are hazardous for the environment and humanity the maximum contamination level (MCL) in the discharged wastewater is set for them. Thus, MCL for nickel is 0.20 mg/L, for cadmium – 0.01 mg/L and for lead – 0.006 mg/L (USEPA). According to Barakat (2011), such concentrations of listed metals boost diseases of circulation and nervous system, brain and kidney damages, dermatitis and nausea. Moreover, they are human carcinogens. To prevent the distribution of these harmful elements in the environment and thus to protect the humanity, efficient, inexpensive and environmentally friendly approach of water treatment should be proposed.

Heavy metal ions can be removed from water by the means of current processes, which include chemical precipitation, flotation, electrochemical deposition and adsorption (Barakat, 2011). Adsorption plays an essential role in the field of water treatment (Largitte and Pasquier, 2016; Ho et al., 2000; Azizian et al., 2009). Due to the ability of adsorption materials to metal binding, adsorption is often used for their removal. Largitte and Pasquier (2016) reported that the adsorption process is widely accepted because it is rather simple, easy to handle, efficient in different conditions and economically viable. However, the disadvantages of this process should be mentioned as well. They are a low selectivity and production of waste products (Barakat, 2011) in the form of used adsorbent containing pollutants.

Among all the different adsorption materials as synthetic and natural materials, industrial byproducts and biological waste, biopolymers are considered very attractive due to their wide availability, high sorption capability and environmental safeness (Barakat, 2011). For this reason, this research focuses on the development a novel biopolymer adsorbent.

1 ADSORPTION THEORY

Adsorption is a process of accumulation of a substance at or near a surface of a sorption material relative to its concentration in the bulk solution. It is necessary to mention that the substance which adsorbs is called adsorbate, and the solid material that accumulates the substance is called an adsorbent (Repo, 2011).

Molecules of a substance are able to locate on the adsorbent surface in two different ways. When each molecule is in contact only with the active site of the adsorbent surface and has no connections with other molecules, it is the monolayer adsorption. In case of presence of several layers of molecules on the adsorbent surface, when not all the molecules are in contact with the adsorbent, multilayer adsorption takes place (Sing, 1985).

As it is rather difficult to determine the exact mechanism of adsorption before the detailed study, generally the process of accumulation of a substance on the material surface is called sorption. According to Ho et al. (2000), sorption process includes different driving mechanism, such as ion exchange, chelation, and physical and chemical sorption. Operation of one or another mechanism depends on the interactions between a sorbate and a sorbent and the complexity of the conditions in the system. Nevertheless, the extent of the interfacial area plays the most essential role in the adsorption process. It corresponds to the specific surface area of adsorbents (Rouquerol et al., 2014). Thus, industrial adsorbents are presented as highly porous materials or materials composed of very fine particles.

1.1. Adsorption mechanisms

Information about the structure and the chemical composition of an adsorbent gives an opportunity for preliminary evaluation of sorption mechanism. For example, if the material has any chemical groups on its surface, that are able to form new chemical bonds due to chemical reactions, the process is called chemisorption. Particularly, acid groups on the sorbent surface form ion exchange sites that are able to accept metal ions or ionic dyes, and amine groups are able to donate a lone pair of electrons for complex formation with metal ions. Sorbents, which does not have any specific functional groups on the surface, are able to provide the physical type of adsorption due to the developed

surface area (Ho et al., 2000). Christmann (2011) reported that chemisorption often occurs on the heterogeneous surfaces while physisorption is more significant in the separation processes near the phase boundaries. Comparison between physical and chemical types of adsorption is represented in the Table 1.

Table1. Physisorption vs. Chemisorption (Zhang, 2016)

Physisorption	Chemisorption
Low heat adsorption (20– 40 kJ/mol)	High heat adsorption (40–400 kJ/mol)
Driving forces: Van der Waal's	Driving forces: chemical bond forces
Occurs at low temperature and decreases with increasing of temperature	Occurs at high temperature
Reversible	Irreversible
Unselective	Selective
Multilayer	Monolayer

Accumulation of molecules can occur on the surface by an ion exchange and chelation as well. Phenomena of ion exchange consists in replacement of equivalent amount of moles of ions from the adsorbent surface by molecules of adsorptive that have the similar charge. Ion exchange as a process is rather quick and can be reversible (Repo, 2011; Loganathan et al., 2013). Chelation poses a bond formation between the binding sites of several molecules around a single united center (Rouquerolt et al., 1994).

1.2. Adsorption kinetics

Adsorption kinetics define the rate of adsorption. It means, how much time is needed to reach the equilibrium between adsorbate on the surface of an adsorbent (or in it) and adsorptive in the bulk solution. This characteristic of the residence time, required to obtain the equilibrium in the system, is extremely important in the field of adsorption process entirely (Ho et al., 2000). Other essential factors are the coefficients related to diffusion, the rate constants (number of molecules or concentration change per time) and the maximum of adsorption (Christmann, 2012; Largitte and Pasquier, 2016).

The behavior of the adsorption kinetics is shown as the loading capacity (q_t, mg/g) versus time (t, min). The formula for the calculation of the amount of adsorption at the

time (the loading capacity) is presented below (eq. 3). An example of the adsorption kinetics plot is presented in Figure 1.

$$q_t = \frac{(C_0 - C_t)}{m_s} \quad (1)$$

where C_0, C_t - concentration of an adsorbate at initial time 0 min and any time t, respectively (mg/L); m_s - dosage of an adsorbent in the solution (g/L).

Adsorption process includes some phases that are characterized by the movement of the ion to the adsorbent and into it. That is why, to understand mechanisms of adsorption process and to discover the rate-determining step, kinetic models should be built. The pseudo-first order and pseudo-second order kinetics models are commonly in use (Repo, 2011).

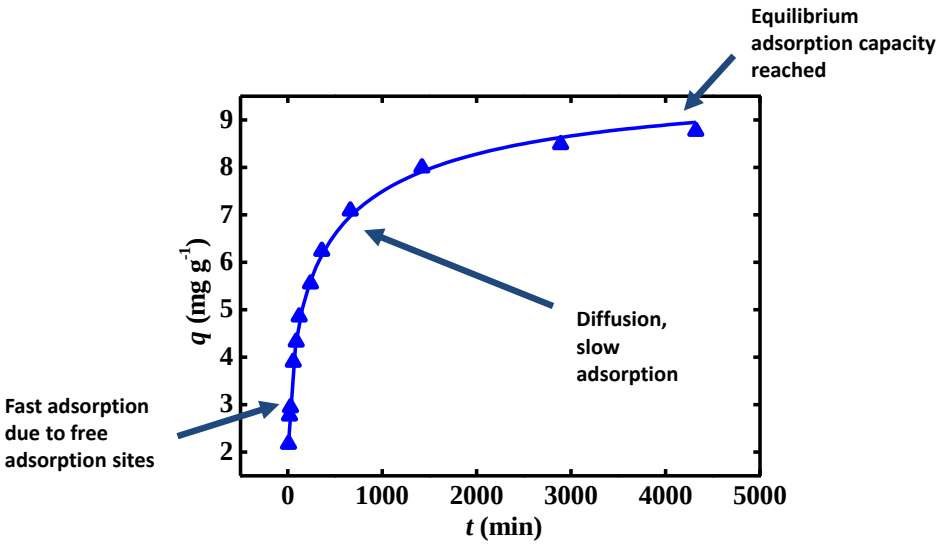

Figure 1. The general adsorption kinetics plot (Repo, 2015).

Suitability of the selected kinetic model will be confirmed by the correlation coefficient between the experimental and theoretical data. The value closest to one will mean that the model provides the best fitting. Both models have linear and non-linear forms. It should be highlighted that transformation of the non-linear equation into linear one lead to errors. That is why it is recommended to use the non-linear form of the model at first to determine the adsorption parameters (Lin and Wang, 2009).

1.3. Adsorption isotherms

Isotherms of adsorption provide information about how much of any substance (adsorptive) can be accumulated by an adsorbent in the particular conditions as pressure and temperature. In other words, an isotherm shows the uptake of adsorptive of a given adsorption material or the efficiency of adsorbent, that is called as adsorption capacity (Christmann, 2011). As a curve, the "isotherm" describes the retention of the substance on a solid surface at various concentrations. It allows predicting the mobility of the substance in the environment (Limousin et al., 2007). The isotherm can be counted completed, when "the solute has reached its saturation value in the solvent" (Giles, 1974). Therefore, adsorption isotherm is the most significant criteria in the adsorption process.

According to IUPAC classification (Sing, 1985), there are six types of isotherms (Fig. 2). Isotherms of Type I are typical for microporous solid materials with relatively small external surfaces. As known microporous solids have pore sizes less than 2 nm. The specificity of microporous materials is that especially pore size regulates the uptake of a substance instead of internal surface area. Examples of such material are activated carbon and zeolites.

Type II is common for non-porous or macro-porous (pore size > 50nm) solids. This type corresponds to unrestricted monolayer-multilayer adsorption. It means that after the monolayer coverage is completed, multilayer adsorption begins. It can be seen from the plot where the starting section of the isotherm transforms into the almost linear middle section (Sing, 1985).

Type III isotherm is convex to the X-axis and quite rarely happens. It confirms unrestricted multilayer adsorption process due to lateral interactions, which are stronger than the interactions between the surface of the material and the adsorbate (Zhang, 2016).

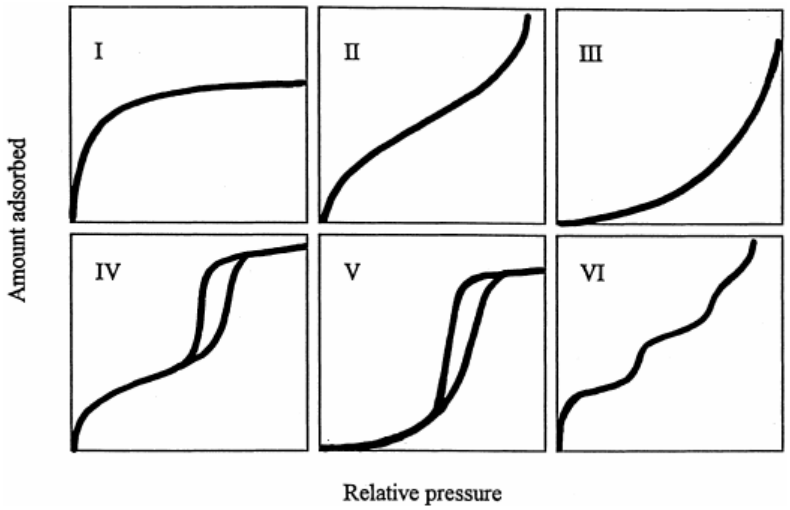

Figure2. The IUPAC Classification of Adsorption Isotherms.

The starting and the middle sections of this adsorption curve Type IV are similar to Type II curve. Therefore, it indicates monolayer-multilayer adsorption process. The final section differs because of another material structure – mesoporous adsorbents with the pore size of 2-50 nm, and it tends to capillary condensation in mesopores. Isotherm of Type V is similar to Type III and corresponds weak interactions between adsorbent surface and adsorbate (Sing, 1985; Zhang, 2016).

Type VI isotherm appropriates to non-porous solids. The stepwise behavior depends on the temperature of the system and indicates monolayer adsorption on each step. Overall, this isotherm corresponds to multilayer adsorption process (Sing, 1985).

Another classification of isotherms is also based on the shape of curves. Charles Giles (1974) firstly observed it. The author divided isotherms of solid solute (Fig. 3) adsorption by their initial slope and classified them into four main classes: S; L ("Langmuir"); H ("high affinity") and C ("constant partition").

The curve "C" passes through the origin. It confirms that the ratio between the concentration of the substance in the solution and its concentration on the solid is the same at any initial concentrations (Limousin et al., 2007). However, practically, it is only possible for systems of very low concentrations (Repo, 2011).

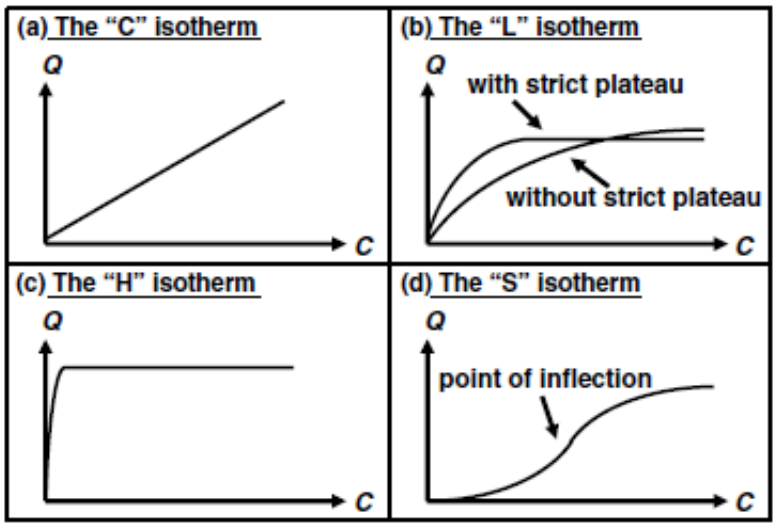

Figure 3. The four main types of isotherms curves (Limousin et al., 2007).

The curve "L" proposes that increase of initial solute concentration causes decrease of the ratio between the remained concentration of the substance in the solution and adsorbed onto the solid surface. This isotherm type also has two sub-group curves. The first one with strict plateau signals that the adsorption material has a limited adsorption capacity. The second one – without a strict plateau, shows the opposite that there is no a defined adsorption capacity (Limousin et al., 2007). According to Repo (2011), this "L" type of the isotherm curve is the most common.

The curve "H" is an isolated incident of the "L" type with a very high initial slope. This tend corresponds to a strong affinity between adsorbate and adsorbent (Limousin et al., 2007; Repo, 2011).

The curve "S" illustrates the low affinity between adsorbent-adsorbate in low solute concentrations. However, after a point of inflection, when some compounds cover the solid surface, other molecules are able to adsorb. This phenomena is also called as "cooperative adsorption" and typical for surfactants (Limousin et al., 2007).

1.4. Biopolymer Nanocomposites as Adsorbent Material

Composite is a material that contains two or more components with different chemical and physical properties. The continuous phase, which is a substrate of a composite, is a matrix. The dispersed phase that is added to a matrix is called a reinforcing agent.

Nanoparticles are often used as a reinforcing material and incorporated into a functionalized matrix (Kumar and Chann, 2015).

Nowadays nanocomposites – multiphase materials in which at least one of the components has one dimension less than 100 nm (Ajayan et al., 2003), are in strong development. They have proven to be a highly potential in adsorption process in the field of water treatment. Removal of different contaminants as heavy metal ions and dyes from wastewater by nanocomposites is attractive due to their tiny size, the absence of internal diffusion resistance and the high ration of surface area to volume (Kumar and Chann, 2015).

The adsorption phenomenon, in the case of composite materials, is not a summative scenario. However, the incorporated material can further improve the substrate, which initially had a good adsorption capacity. For example, if initially an adsorption phenomenon is based on the surface forces as hydrogen bonding or electrostatic interactions, the final adsorption capacity could be almost considered as a sum of the original properties of the composite sources (Terzopoulou et al., 2015). Therefore, as the result, the synthesized nanocomposite will own more significant properties than the individual component parts (Sampath et al., 2016).

It was found that metal oxide nanoparticles, based on aluminum, titanium, magnesium, cerium, and ferric, provide a high efficiency for pollutants removal from water solutions. That is why they are used as reinforcements in nanocomposite materials (Kumar and Chann, 2015).

As it was mentioned above, typical reinforcement agents are metal oxide nanoparticles and that biopolymer materials are highly attractive as a matrix for nanocomposite. Biopolymers are 100% renewable and biodegradable polymers (Dufresne et al., 2013; Jawaid et al., 2017). The main features of biopolymers, that can be very attractive for adsorption process, are existence of a number of different functional groups in the structure of such materials. Presence of functional groups is able to increase adsorption efficiency for the removal of metal ions from aqueous solution (Barakat, 2011). The sorption mechanism in this case typically is a precipitation of metal ions by chemisorption or chelation (Pérez et al., 2006).

It should be mentioned that biopolymer matrices are obtained from renewable sources and that is why a production of this type of adsorbent is a step for minimization of the environment impact. Moreover, bio based materials are the best alternative to synthetic ones because their utilization is more economical (Dufresne, 2013). Cellulose, chitin and chitosan, lignin and other natural polymers can be used as biopolymers for nanocomposite matrix. However, among the currently used biopolymers as a matrix for nanocomposite adsorption materials, lignin has variety of advantages and specific characteristics, as amorphous structure (Thomas and Visakh, 2012) and chemically reactive groups that form sites for chemical modifications (Dufresne and Thomas, 2013). This makes it highly attractive for further research in the field of adsorption. Listed properties also correspond to using lignin as a hydrogel, antioxidant, thermosetting and thermoplastic polymer composites, lignin-reinforced and lignin-based nanocomposites and so on (Tian et al., 2017).

1.4.1. Lignin

Vainio (2007) reported that lignin is a side-product, which remains in the result of not complete utilization of biomass. In other words, it has not direct productive value and tons of by-products have remained. With reference to lignin, it has a high prospective in further use, and especially from ecological point of view, because it is renewable and biodegradable material (Thomas and Visakh, 2012), and it functions in scopes of a trend of minimization of wastes and involvement of by-products into a manufacture.

Lignin can be isolated from wood and plants by different industrial processes (Thomas and Visakh, 2012). Thus, lignosulfonates and Kraft (soda) lignin are the result of sulfite and sulfate pulping, respectively. Due to acidic processes such as acidic hydrolysis lignin is produced. Other methods for lignin isolation are water and steam treatment, mechanical wood milling and treatment with organic solvent mixtures. All processes promote the production of lignin of different composition and properties. Moreover, the source of lignin (wood or plants) and methods of treatment and modification after isolation influence on the product.

Lignin is found as high heterogeneous phenolic polymer including a network of three-dimensional aromatic and aliphatic fragments (Thomas and Visakh, 2012). Lignin is

also known as a highly reactive compound due to its functional groups – aromatic rings, phenolic, aliphatic alcohol and methoxy groups, that are oxygen –bearing groups and presents as active sites for metal ions adsorption and other substances (Pérez et al., 2006). In accordance with polymer length, the molecular weight of lignin can vary from 2000 to 15000 g/mol. Lignin is also resistant to chemical reactions, however, it can be mechanically cleavable to low molecular weight. It should be mentioned that lignin is not soluble in water (Celik and Demirbas, 2005), that makes it suitable for use in the water environment.

1.4.2. Hydrolysis lignin

In this research hydrolysis lignin is used as a biopolymer matrix for nanocomposites synthesis. Hydrolysis lignin is a large-tonnage waste after wood percolation with diluted sulfuric acid in bio-ethanol production (Hatakeyama, 2009; Popova et al., 2015). The percolation hydrolysis is realized at high pressure (0.6 – 0.9 MPa). The temperature of the process is around 200 ^{o}C. Condensation, oxidation, and demethylation take place in the acidic environment and accompany this process. As the result, in comparison with the original lignin structure, the acidic lignin molecule includes fixed benzene rings (Popova et al., 2015).

Nowadays, hydrolysis lignin presents a special attention as organic natural sorbent (Po et al., 2016). Due to bipolar structure of the hydrolysis lignin, it is able to accumulate pollutants such as heavy metal ions via ion exchange, chelating, chemisorption, and physical sorption (Efimova et al., 2017).

1.4.3. Removal of heavy metal ions by lignin and lignin-based composites

Celik and Demirbas (2005) reported successful results of using modified lignin from pulping wastes in the case of removal heavy metals. The maximum adsorption capacities for Zn(II) were 11.3 mg per g of the lignin, and 17.5 and 7.7 mg/g for lead and cadmium, respectively. Berrima et al. (2016) converted lignin precipitated from black liquor into a charcoal by pyrolysis. Obtained charcoal was used for the removal of Pb(II), Cd(II), Hg(II) and Ni(II) from aqueous solutions. The tests showed that the obtained material had high adsorption capacity that ranged from 200 to 600 mkmol/L depending on a metal ion. Pérez et al. (2006) also reported about a high adsorption capacity of lignin

precipitated from black liquor in the case of Ni and V ions removal. Efimova et al. (2017) reported a study about suitability of hydrolysis lignin in the case of Cu(II), Zn(II), Ni(II) and Co(II) adsorption from the solutions with different pH ranges.

However, properties of lignin can be enhanced via some reinforcement agents. Synthesis methods for modification of biopolymer into reinforced nanocomposite material are direct ion exchange and co-precipitation (Darder et al., 2005). In other words, intercalation of additional groups is applied in order to improve the properties of nanocomposites. One of the methods for reinforcing lignin is a precipitation of metal hydroxide nanoparticles on its surface. Thus, Tian et al. (2017) reported a study about a precipitation method for preparation of lignin-based (lignin/silica) nanocomposite. According to conducted tests, the synthesised material obtained well-defined dispersive, morphological and adsorption properties. SEM and BET results confirmed a porous structure with a great surface area. According to Feldman (2016), lignin-based carbon/$CePO_4$ nanocomposite material was able to be synthesized via a hydrothermal technique with mixing a lignin suspension with a metal salt solution.

In this study, a novel lignin-based nanocomposite was obtained from hydrolysis lignin via co-precipitation method. Magnesium hydroxide was chosen as a reinforcing agent because it is one of the most promising additives (Ponomarev, 2017). Brucite itself is white and is represented as an axialite structure (layer-like crystal structure) or fibrous structure. Izotov (2002) observed sorption properties of brucite in a relation of heavy metal ions. Therefore, brucite as a reinforcing agent is a highly suitable to be applied in the heavy metals adsorption process.

2 ANALYTICAL METHODS FOR CHARACTERIZATION OF ADSORBENT

2.1. Determination of the SSA via BET method

The specific surface area including pore size distribution can be calculated in accordance with BET (Brunauer, Emmett, and Teller) adsorption isotherm equation. Method BET takes into account the physical gas adsorption onto the solid surface. This gas adsorption method also allows determining the size and volume distribution of micropores. Information about the specific surface area is used to predict dissolution rate and bioavailability (Particle Analytical, 2017).

Sample preparation for the analysis involves preparing a sample of a certain mass with an accuracy of 0.0001 g (the recommended weight of the sample is 100 mg). The sample is placed in a special analytical tube and send for degassing. In this study, degassing was carried out at 300 ^{o}C in a vacuum for 2 hours. After degassing, the mass of the material is determined and tubes with degassed samples are fixed in the ports of the device. Compressed helium and nitrogen are used to determine the BET specific surface.

Gas-adsorption analyzer is used for this analysis. The principals of operating the device includes the study of a static sorption of nitrogen vapors at boiling temperature (77 K). Other words, the amount of adsorbed substance in accordance of decreasing of adsorbate in a vapor phase is determined. The analysis is carried out in a hermetical reactor filled with gas or steam at a certain pressure. Under such conditions, the tested material accumulates the gas, and, correspondingly, its mass increases, and the pressure of the gas phase in the device decreases. After a while the system reaches equilibrium, i.e. the adsorption material obtains a constant mass, and the pressure becomes constant. The amount of adsorbed nitrogen and, accordingly, the pore size of the material, is calculated by the reducing of pressure in the device (Fedin, 2014).

2.2. Fourier Transform Infrared Spectroscopy (FTIR)

FTIR is an analytical method for identification of organic and, more rarely, inorganic materials. This method allows determining molecular components and structure of the sample material due to infrared absorption bands. Irradiation of a sample material causes high vibrations of its molecules. A particular molecule absorbs a defined wavelength that is a function of energy difference within the at-rest and excited vibration states.

Thus, each wavelength absorbed by a sample material is characteristic of its molecular structure. The result of measurement is represented as a plot of absorption intensity (or percentage of light transmittance) versus wavelength (or more specifically wave number in cm^{-1}) (Hanke, 2001).

Identification of the unknown IR spectrum is carried out by comparison with standard spectra in software database or with a spectrum of the known material. Adsorption bands that occur in the range of 1500 – 4000 cm^{-1} characterize typical functional groups of the material. Wavenumbers from 400 to 1500 cm^{-1} are known as the fingerprint region, which is very specific (Hanke, 2001).

2.3. Inductively Coupled Plasma Optical Emission Spectrometry (ICP-OES)

ICP-OES is able to determinate elements in a numerous of samples at a short time. The operation principle includes an injection of a liquid sample into induced argon plasma using a nebulizer. When the sample reaches the plasma, it quickly vaporizes and energizes due to an extremely high temperature 5000-7000 K (Hou and Jones, 2000). Emission (spectrum) rays release when the excited atoms return to at-rest state. Emission rays are determined and measured via array detector and corresponded to the photon wavelength. The type of element can be identified due to the position of photon rays, and the element concentration – due to the rays' intensity (Hitachi, 2017).

2.4. Transmission Electron Microscopy (TEM)

TEM provides morphological, compositional, and crystallographic information of samples. TEMs are the most powerful microscopes. Maximum potential magnification of TEM is one nanometer. Therefore, they are appropriate to get images of the microstructures (particles, microcracks, and micropores). TEM consists of an electron gun that produces electrons. Magnetic condensing lens condenses electrons to a beam and regulates the size of electrons fold on the specimen. The specimen is located on the sample stage between the condensing lenses. For this analysis, samples should be prepared very carefully. They should be chopped to very thin that gives them a property known as electron transparency (Microscope master, 2017).

Due to the magnetic condensing lens a stream of electrons, produced by the electron gun, fall over the specimen. Electrons pass through the specimen and form an image. The device is able to produce two-dimensional, black and white images in a high resolution. The light areas of the image mean the places where many electrons passed through the sample. In contrast, the dark areas represent dense areas of the sample, which can be presented as particles and other impurities. The combination of light and dark areas provides the information of the structure, texture, shape, and size of the tested material (Microscope master, 2017).

2.5. Thermal analyses

Physical and chemical changes in a material as a function of temperature can be determined via thermal analysis. Such changes in a material are caused by dehydration, decarburization, melting, crystallization etc. Thermal analysis includes two basic methods, which are DSC (differential scanning calorimetry) and TGA (thermogravimetric analysis). They are commonly used for the detection properties of organic polymers. There is the third method that is similar to DSC, it is DTA (differential thermal analysis). The difference between them is the use of a higher temperature. Thus, typical temperature in DSC is -50 ^{o}C to 300 ^{o}C, and for DTA – greater than 1500 ^{o}C. That is why DTA is more appropriate for metals, ceramics, and glasses. Typical requires for these methods are 6 – 10 mg of a sample for DSC and DTA, and 20-30 mg for TGA. Solid or liquid samples are admitted. Measurements are carried out in presence of inert gas (Hanke, 2001).

2.5.1. Thermal Gravimetrical Analysis (TGA)

In TGA, the weight of the sample is continuously measured as a function of time and temperature. These measures are performed when a sample is placed in a small pan, which is connected to a microbalance and a heater. The change of weight in given time and temperature is recorded. These changes can also be detected as a rate of weight loss. The obtained data of weight change in specific time is correlated with reactions occurring in a sample (volatilization of some components of a sample, oxidation or reduction and so on). Some thermal events as melting and similar ones cannot be detected if there are no changes in sample mass (Hanke, 2001).

2.5.2. Differential Thermal Analyses (DTA)

DTA measures heat flow to or from a sample as a function of temperature and time. These measures are performed in a small pan under heating or cooling conditions. A reference material also undergoes these temperature changes. Then differences in temperature between a sample and a reference material are determined as the same amount of heat energy is added to both. This method provides the information of melting temperature, glass transition temperature, and others. DTA also can be used for detecting the temperatures of solid-state transformations (Hanke, 2001).

2.6. X-Ray Powder Diffraction (XRD)

XRD is a rapid analytical method that allows identifying the crystalline phase of the material and atomic spacing that makes possible to define the unknown crystalline material. Max von Laue (1912) reported that crystalline substances act as three-dimensional diffraction gratings for X-ray wavelength, which are analogous to a space between planes of the crystalline grid. Constructive interference of monochromatic X-rays and a crystalline sample are the basis of XRD. X-rays are generated in a cathode ray tube by heating, then filtered until produce of monochromatic radiation and by applying a voltage (for accelerating an electron stream) bombardier to the tested material (Dutrow et al., 2017).

X-rays fall on the sample surface at a certain angle. Constructive interference is created when values of wavelength and the angle satisfy Bragg's law ($n\lambda=2d \sin \theta$). Bragg's law connects the wavelength (λ) of X-ray, to space (d) between planes of the crystalline grid and the diffraction angle (θ). During the scanning of the sample through the range of 2θ angles, all possible directions of the crystal grid should be reached due to accidental positions of the sample material in a diffractometer. The turns of the sample are provided by a goniometer. Diffraction peaks correspond to d-spacing of a crystalline grid of the material. As d-spacing is a specific feature of the material, it makes it possible to identify the material by comparison with standard reference patterns. The value of 2θ angles for typical reference patterns are 5^o – 70^o. Results of the analysis are represented as a diffractogram of counts per second (Y-axis) vs. degrees 2θ (X-axis) (Dutrow et al., 2017).

3 OBJECTIVES AND STRUCTURE OF THE WORK

This research consists of several aims. The first one is the synthesis of a novel biopolymer nanocomposite based on lignin and magnesium hydroxide as a reinforcing agent. Synthesized material (LH-MH) was granulated in order to improve its usability and one part of the obtained material was transformed into a coal (LH-MH-450) by pyrolysis. Thus, two adsorption materials were produced. Therefore, the second objective of the research aims to define the structure and the composition features via current analytical equipment and to compare both materials with each other.

As the primary target of the research is development an adsorption material for the removal of heavy metal ions (Ni(II), Cd(II), Pb(II)) from aqueous solution, general adsorption properties of obtained LH-MH and LH-MH-450 were investigated in different experimental conditions. The effect of pH and pH_{zpc}, temperature, contact time, and initial metal concentration were studied for both of them. Removal of Ni(II), Cd(II), Pb(II) from the multicomponent system and in the presence of competitive ions was conducted for establishing more real conditions of the adsorption process. Desorption study for both materials was conducted as well.

The fourth aim was to suggest a mechanism of adsorption phenomena that take place with the use of obtained biopolymer nanocomposites. For this reason, isotherm and kinetics models were analyzed. As the last step, the comparison based on contact time study between novel synthesized adsorbents LH-MH and LH-MH-450 and commercially used granulated activated carbon Norit EA 0.5-1.5 was realized.

4 MATERIALS AND METHODS

Commercially available hydrolysis lignin for the research was obtained from Russia. In a result of the gravimetric analysis, the moisture content of lignin was about 67%. Chemicals used for the solution preparation in this study were of analytical grade and provided by Sigma-Aldrich. Sodium hydroxide 10% solution for synthesis was prepared by dissolving 50 g of NaOH in 500 ml volumetric flask by double deionized water. For the preparation of 1 M magnesium chloride solution 203.21 g of $MgCl_2 \cdot 6H_2O$ was dissolved in 1 L of double deionized water. Working solutions of Ni(II), Cd(II), Pb(II) ranging from 0.1 to 25 mmol/L for adsorption tests were prepared by dilution of 0.1 mol/L stock solutions. Stock solutions were prepared by dissolving the calculated quantity of Ni(II), Cd(II), and Pb(II) nitrate salts. Nitrate salts of Na, K, Mg(II) were used for the test with competitive ions. pH correction in the solutions was realized by 0.1 M NaOH and 0.1 M HNO_3 and measured by pH-meter.

The equipment for synthesis process is shown in Figure 4. Separation of synthesized material from the bulk solution was obtained with the centrifugal machine (Eppendorf 5810). The slurry was washed on a Buchner funnel and Bunsen's flask. TERMAKS oven was used for drying the obtained material. Grinding of the dry material was carried out by a pestle. Conversion of synthesized LH-MH to LH-MH-450 (coal form) was realized in a pyrolysis furnace. For the adsorption batch tests plastic tubes (50 mL) and an orbital shaker (IKA KS 400), syringes (10 mL) and PTFE membranes (0.45 µm) were used.

Textural properties and, particularly the specific surface area were examined via N_2 adsorption/desorption isotherms (BET method). Morphology, crystalline structure, and characteristics of surface chemistry were investigated via TEM, XRD and FTIR, respectively. Thermal stability and thermal events were analyzed from TG and DT curves. The pseudo-first-order and pseudo-second-order kinetics models and the Langmuir and Freundlich isotherm models were used for simulating the adsorption process.

4.1. Synthesis of lignin based nanocomposites

Synthesis of LH-MH

Hydrolysis lignin was reinforced by magnesium hydroxide via co-precipitation method to improve its adsorption properties. Proportion between dry lignin and $MgCl_2$ was chosen as 1:1. The experiment was carried out under mixing conditions, and the temperature of the suspension was maintained at 60 ℃ over the whole period. Thus, 27.78 g of hydrolyzed lignin (undried) was mixed with 200 mL of 10% NaOH at 300 rpm of agitation during 1 hour. After this time, 102 mL of magnesium chloride was added dropwise to the suspension, and stirring was increased to 700 rpm for 16 hours under the installed temperature.

Figure 4. The synthesis unit.

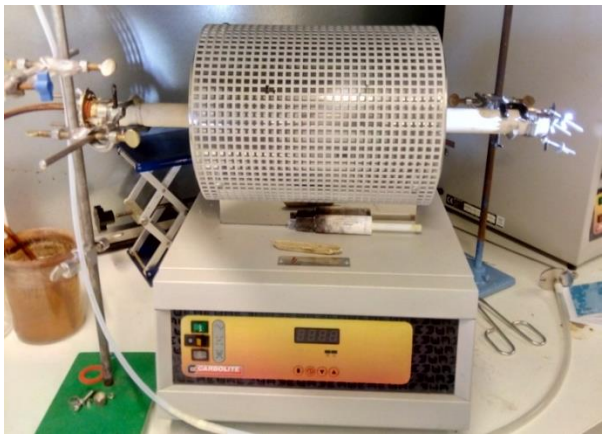

Figure 5. The pyrolysis furnace.

The obtained slurry was separated by centrifugation at 700 rpm for 12 min. Then separated solid was mixed with 200 mL of 10% HCl and washed 5 times by boiling water on Buchner funnel until acid traces were not detected by litmus paper. Washed material was granulated by piston type granulator and dried in the oven at 70 ^{o}C for 16 hours. After this time, the dry material was gritted via mortar and pestle up to the size

of granules around 3 - 5 mm. In the result of the synthesis, around 10 g of the material was obtained.

Synthesis of LH-MH-450

Synthesis of this material has the same stages as the synthesis of LH-MH. However, granules after preparation were carbonized in a pyrolysis furnace (Fig. 5). The process was carried out for 90 min at 450 ^{o}C. The heating rate was installed as 7 ^{o}C per minute.

4.2. Characterization of LH-MH and LH-MH-450

Characterization of obtained materials was studied via different analytical methods. Determination of the materials' chemical structure and formation of additional functional groups due to synthesis process were carried out by FTIR (Bruker Vertex 70). Determination of the crystalline part of the structure of the material was defined by XRD (PANalytical). Changes of the material (thermal decomposition) as a function of time and temperature were detected by TGA and DTA. The specific surface area of the materials was estimated by BET (Tristar® II Plus). The morphology of the materials was analyzed with TEM (Hitachi H-7600).

pHzpc of synthesized LH-MH and LH-MH-450 was also determined.. Sample weights of both materials were added to 0,01 M NaCl solutions of different pH range from 2 to 12 for 48 hours for this test. After this time, the final solutions were measured with pH-meter. Obtained results are presented as a graph between initial and final pH. The point of intersection between these curves will be pH_{zpc} of the adsorbent samples.

4.3. Adsorption tests

4.3.1. Batch adsorption tests

For the deepest study of the obtained materials, adsorption tests for the removal of nickel, cadmium, and lead were performed. The working solutions of these cations were 0.5 mmol/L (or 58.7; 112.4 and 207.2 mg/L for Ni(II), Cd(II), and Pb(II) respectively). All tests were carried out in the plastic tubes (50 mL) in mixing conditions on an orbital shaker. The optimal sample weight was estimated as 80 mg. Batch adsorption study was

conducted during 16 hours at room temperature. Uptake (q, %) of ions of interest via tested adsorbents was calculated as:

$$q = \frac{(C_i - C_e)}{C_i} \cdot 100\% \quad (2)$$

To determine the equilibrium adsorption capacity (q_e) the following formula was used:

$$q_e = \frac{(C_i - C_e)}{m} \cdot V \quad (3)$$

where C_i and C_e are the initial and the equilibrium concentrations (mmol/L); m is the sample weight of tested adsorbent (g); V is the volume of the solution (mL).

The first one of the adsorption tests was determination of an optimal dose of the adsorbent. In this case, sample weights from 20 mg to 160 mg for both LH-MH and LH-MH-450 were prepared. All doses of the adsorbents were tested in 40 mL solutions of Ni(II), Cd(II) and Pb(II). After the optimal dosage was found, the second test of pH study was taken. Solutions of ions of interest in a range of pH 1- 8 were checked. For determining the optimal thermal conditions adsorption tests were carried out in the range of temperatures between 25 and 65 ^{o}C.

The effect of contact time was also studied for the removal of heavy metal ions by the adsorbent materials and by the commercial activated carbon. Ten time slopes in the range between 5 and 1440 minutes were chosen. At each time slot, the solution samples were taken out and filtered by the PTFE membranes (0.45 μm), and then analyzed by ICP.

Initial concentrations of 0.01 – 25 mmol/L of the solutions for the isotherms modeling were chosen. Adsorption batch tests were carried out with optimal amount of adsorbents and during 16 hours, that was enough to obtain equilibrium.

Multicomponent solutions were prepared for the analyzation of capability of LH-MH and LH-MH-450 to act in work in the multicomponent system and in the presence of competitive ions. One of the solutions contained Ni(II), Cd(II) and Pb(II) in equal portions, and the other one included the listed ions plus K, Na, and Mg(II).

Desorption of adsorbed metal ions was carried out by 0.1 M HNO_3 and by washing with DI water. The process was repeated two times. The desorbed concentration of Ni(II), Cd(II) and Pb(II) was examined via ICP after each test.

4.3.2. Adsorption kinetics

Kinetics study for LH-MH and LH-MH-450 was performed. Obtained data for the kinetics study is presented in the appendices IV. Pseudo-first-order and pseudo-second models were used for identification the rate of the adsorption of Ni(II), Cd(II) and Pb(II) onto the LH-MH and LH-MH-450. Both models can be presented in the linear and non-linear form. Linear forms of the models are derived via linearization of the basic equations 5 and 8. The value of the equilibrium adsorption capacity (q_e) (eq. 7) was taken from the plot of equilibrium adsorption study (Fig. 21). The rate constants (k_1 and k_2) can be found from the slope of the line, and the equilibrium (q_e) – from the intersection point. The method of ERRSQ (the sum of the square of the errors) was used for evaluating the unknown parameters of the kinetic models. This method allows minimizing the difference between experimental data and theoretical calculations. The sum of the square of the errors is calculated as shown in equation 4. It was carried out by Solver Application of the MS Excel.

$$\sum_{i=1}^{n}(Q_{e.exp} - Q_{e.theor})^2 \quad (4)$$

where $Q_{e.exp}$ and $Q_{e.theor}$ are experimental and theoretically calculated adsorption capacity (mg/g).

4.3.2.1. Pseudo-first-order model

The presented model was proposed by Lagergren (1898). However, only in 1990 this model was used in the case of Ni(II) removal by wollastonite by Sharma et al. (1990). The main suggestion of the model is that there are no interactions between ions and each ion sorbs on a local site. The model also approves that the coverage does not influence on the adsorption energy and the concentration of a substance is constant. This theory designs the adsorption process as a monolayer of adsorbate on the adsorbent surface (Largitte and Pasquier, 2016). Equation 5 represents the pseudo-first order model (PS1).

Linear and non- linear forms of the PS1 model (eq. 6-7) are obtained by integration the initial equation 5 by using the boundary conditions: $q_t = 0$; $t = 0$; $q = q_t$ at $t = t$ (Lin and Wang, 2009).

$$\frac{dq_t}{dt} = k_1 \cdot (q_e - q_t) \quad (5)$$

Non-linear var.: $q_t = q_e \cdot (1 - \exp(-k_1 \cdot t))$ (6)

Linear var.: $\log(q_e - q_t) = \log(q_e) - \frac{k_1}{2{,}303} \cdot t$ (7)

where q_e and q_t are equilibrium (maximum) adsorption and adsorption per time, (mg/g; mmol/g); k_1 - rate constant, (min^{-1}).

4.3.2.2. Pseudo-second-order model

Blanchard et al. (1984) proposed the equation for the second-order model. Initially this model was used to describe the removal of heavy metals from water by zeolites. The presumptions of the second model look like the suggestions of the first one. However, the main difference between them is using the second-order rate in the equation. It should be mentioned, that the pseudo second order rate constant is equal to the initial concentration of a substance in a solution (Azizian et al., 2009). Equation 8 represents the pseudo-second order model (PS2). The linear and non-linear forms of the model were obtained by the integration of the initial equation.

$$\frac{dq}{dt} = k_2 \cdot (q_e - q)^2 \quad (8)$$

Non-linear var.: $q_t = \frac{q_e^2 \cdot k_2 \cdot t}{1 + q_e \cdot k_2 \cdot t}$ (9)

Linear var.: $\frac{t}{q_t} = \frac{1}{k_2 q_e^2} + \frac{1}{q_e}$t (10)

where q_e and q_t are equilibrium (maximum) adsorption and adsorption in each time moment, (mg/g; mmol/g); k_2 – the second-order rate constant, (g/mg min).

4.3.3. Isotherm models

There are a lot of different isotherm models that help to estimate chemical and physical properties of the material, and also to understand how adsorption process goes on a

given surface. Fitting of adsorption isotherms depends on the nature of the adsorbent and the interactions between it and a substance of interest (Christmann, 2011). Originally, isotherms were theoretically depicted for the gas/solid interactions. However, they were lately modified for the solid/liquid system via replacement of relative pressure to equilibrium concentration (Repo, 2011).

Langmuir and Freundlich isotherm models are the most common in use mainly because they contain only two parameters and are easily fitted to experimental data (Repo, 2011). So, these models were used for analyzation of the experimental data (appendices V). To evaluate the unknown parameters of the isotherm equation the error solution method (ERRSQ) was used and realized by means of Solver MS Excel. The plots of the Langmuir and Freundlich isotherms are illustrated in Figures 24 - 25, and the constants are presented in Table 6.

4.3.3.1. Langmuir isotherm model

The theoretical Langmuir equation (eq. 11) was proposed in 1918 for the adsorption of gases onto the solid surface (Langmuir, 1918). The theory of Langmuir isotherm model assumes that adsorbent has a homogeneous surface and so the energy of all adsorption sites is constant. It also predicts local adsorption. In other words, each adsorption site is able to accumulate only one adsorbate. The non-linear form of the Langmuir isotherm that is also suitable for liquid-solid system can be expressed as equation 11 (Repo, 2011).

$$q_e = \frac{q_m K_L C_e}{1 + K_L C_e} \tag{11}$$

where q_e - the adsorption capacity, (mg/g); C_e – the equilibrium concentration of the adsorbate (mg/L); q_m - the maximum adsorption capacity of adsorbent (mg/g); K_L- the energy of the adsorption (L/mg).

4.3.3.2. Freundlich isotherm model

This model was proposed by Freundlich in 1906. As well as Langmuir isotherm, Freundlich isotherm includes two parameters. However, it takes into account

heterogeneous adsorption surface that consist of sites with different adsorption energies (Repo, 2011). Non-linear form of the model is presented below:

$$q_e = K_F C_e^{1/n_F} \quad (12)$$

where q_e - the adsorption capacity, (mg/g); C_e – the equilibrium concentration of the adsorbate (mg/L); K_F and n_F - the Freundlich adsorption isotherm constants.

4.4. Analysis of solutions

Samples of the solutions after adsorption batch tests were picked out by syringes (10 mL) and filtered by PTFE membranes (0.45 μm). To take into account the range of possible concentrations for ICP-OES, samples of the solutions with high concentration of metal ions were diluted for 2 and 10 times. Control of adsorption properties of the materials (LH-MH and LH-MH-450), in particular, initial and final metal concentration in solutions, was checked by ICP-OES (Thermo iCAP 6300 series). The used wavelengths for Ni(II), Cd(II) and Pb(II) were: 216.6 nm; 214.4 nm and 217.0 nm respectively. For the test in presence of competitive ions the following wavelengths were used: Ca(II) – 393.4 nm; K– 766.5 nm; Na – 588.6; Mg(II) – 279.6 nm.

The concentration of the solutions with ions of interest before and after adsorption process was estimated using the calibration curves. Calibration solutions were prepared from the standard solutions (especially for ICP use). The calibration curve included the following points: 0.5; 1; 5; 10; 30; 50 mg/L. The point of a quality sample (QS) was chosen as 25 mg/L. The necessary volume of the standard solutions with concentration 1000 and 10000 ppm was calculated in accordance with the equivalent law (eq. 13), and was dissolved by 10% HNO_3:

$$C_1 \cdot V_1 = C_2 \cdot V_2 \quad (13)$$

where C_1, V_1 – the concentration and the volume of desired solution; C_2, V_2 – the concentration and the volume of standard solution.

5 RESULTS AND DISCUSSION

As a main result of the experiments, a novel biopolymer nanocomposite based on lignin was obtained. The illustration of both obtained materials is presented in the Figure 6. LH-MH, synthesized firstly, is on the right side. It is brown. LH-MH-450 represents a pyrolysis modification of LH-MH, and because of the temperature treatment, it is black. The size of the granules is around 3-5 mm. The granules were mechanically resistant, held their shape and did not decay in water.

Figure 6. The synthesized nanocomposite materials: a) LH-MH-450; b) LH-MH.

5.1. Characterization of LH-MH and LH-MH-450 via analytical methods

5.1.1. Parameters of porous structure via BET method

Parameters of the porous structure of synthesized biopolymer nanocomposites LH-MH and LH-MH-450 were estimated by modeling nitrogen adsorption-desorption isotherms via BET method, average characteristics of pores as volume and width were detected via BJH method. The obtained results are presented in Table 2. Pores of both materials correspond to mesopores in accordance with IUPAC classification.

Table 2. Adsorptive properties of the biopolymer nanocomposites

Sample	BET Surface Area (m^2/g)	BJH pore volume (cm^3/g)		BJH average pore width (nm)	
		Adsorption	Desorption	Adsorption	Desorption
LH-MH	32.7	0.09	0.09	11.0	7.2
LH-MH-450	20.6	0.06	0.07	16.2	8.4

The results demonstrate that LH-MH had the higher specific surface area and volume of pores than LH-MH-450. Furthermore, the pore sizes of LH-MH-450 were larger. It means that the heat impact during the pyrolysis promoted the increase of pore size and,

consequently, the decrease in surface area. In comparison with the results of Pérez et al. (2006) and Tian et al. (2017), the measurements of BET surface area of lignin was 1.37 and 7.13 m^2/g respectively. Thus, it is possible to say, that improvement of lignin by the modification made the synthesized materials more appropriate for adsorption process.

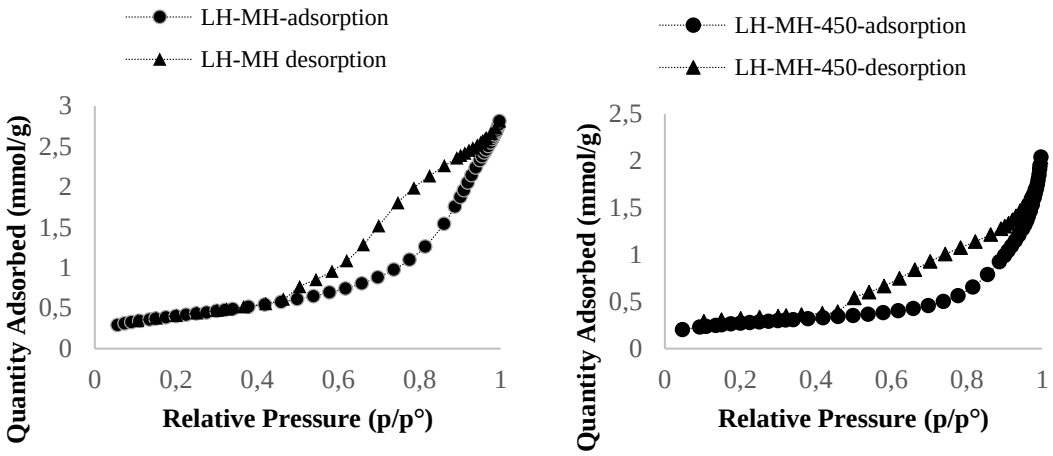

Figure7. Nitrogen adsorption-desorption isotherms of LH-MH and LH-MH-450.

Figure 7 illustrates the nitrogen adsorption-desorption isotherms of LH-MH and LH-MH-450. The lower portion of the loops corresponds to the adsorption process. They also resemble the type III isotherm in accordance with IUPAC classification. This confirms unrestricted multilayer adsorption process.

5.1.2. Surface characterization via FTIR

FTIR analysis was taken in order to identify the functional groups in the structure of the synthesized nanocomposites. FTIR spectra of LH-MH (lignin reinforced by brucite) and LH-MH-450 (material after heat treatment) are presented in the Figures 8 and 9.

Figure 8 confirms the presence of brucite in the structure of the synthesized nanocomposite LH-MH via the strong peak at 3699 cm^{-1}, which corresponds to $Mg(OH)_2$ lattice vibrations (Ponomarev et al., 2017). This peak is not found on the LH-MH-450 curve, which confirms decomposition of brucite at a high temperature. The methylene group, which corresponds to anti-symmetric stretching and represents as the peak at 2926 cm^{-1} (Tian et al., 2017) on the LH-MH curve, decomposes after the temperature impact, and thus, the peak is absent on the LH-MH-450 curve. Broad peaks at 3383 cm^{-1}

and 3357 cm^{-1} on the LH-MH and LH-MH-450 curves respectively correspond with water molecules vibrations. Thus, these peaks belong to stretching vibrations of O−H groups. However, the peak on the LH-MH-450 is less intensive compared to that on LH-MH. It shows the evaporation of water molecules during the heat treatment.

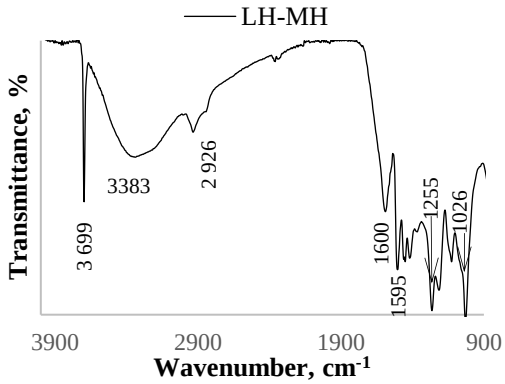

Figure 8. FTIR spectra of LH-MH.

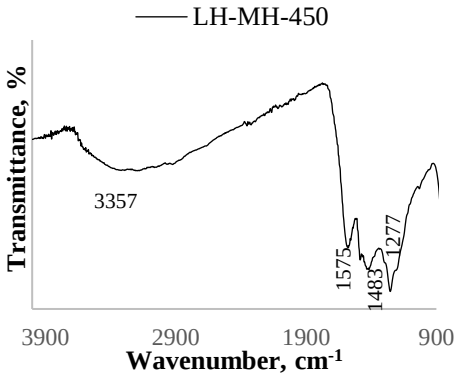

Figure9. FTIR spectra of LH-MH-450.

Nevertheless, skeletal vibration modes of the benzene ring, represented at 1575-1600 cm^{-1}, and vibrations of aromatic rings at 1483cm^{-1}(Tian et al., 2017), are on the both LH-MH and LH-MH-450 curves. The peaks at 1255 cm^{-1} , 1026 cm^{-1} (Fig.8), and 1277 cm^{-1} (Fig.9) identify the C=O vibrations and C-O deformation vibration of primary alcohols, respectively (Karmanov and Derkacheva, 2012).

5.1.3. Thermal analysis

TG and DTG curves were analyzed to estimate the thermal events happening with tested samples. Based on TG curve it is possible to examine the change of mass as a function of increasing temperature. Thus, according to the Figure 10, the first mass change of sample occurs until 260 ^{o}C and consists of 14% of the initial sample mass. 73% mass change happens in the range of temperatures of 260 – 525 ^{o}C. After the second mass change, the system reaches the equilibrium. Nevertheless that the weight loss of both materials happens almost parallel, the inorganic part (ash) content in the sample is 12.6% in LH-MH and 17.2% in LH-MH-450. Such a difference in the ash content in the samples is because LH-MH-450 was exposed by high temperature earlier and some organic part was converted into an ash.

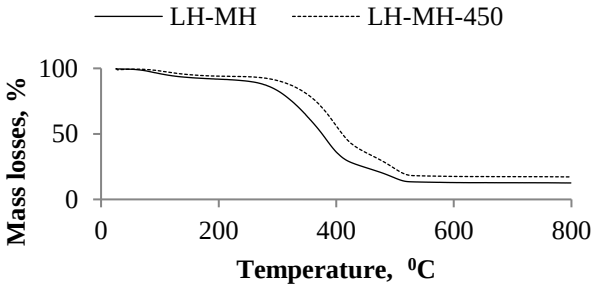

Figure 10. TG curve of LH-MH and LH-MH-450.

DTG is a derivate of TG. DTG curve (Fig. 11) represents a rate of change of the sample mass, and DTA curve allows determining of endothermic and exothermic events. The first endothermic peak at 92 ^{o}C (DTA curve) and the peak at 102 ^{o}C (DTG curve) related to water liberation (Darder et al., 2005). The initial temperature of lignin degradation is 190 ^{o}C (Xiao et al., 2013). Tian et al. (2017) reported about the degradation of lignin structure in the temperature range between 200 ^{o}C and 600 ^{o}C. According to Darder et al. (2005), a partial dihydroxylation of the brucite lattice occurs in the range of temperatures between 200 and 450 ^{o}C. So, it is possible to make a conclusion, that thermic peaks of lignin and brucite structure coincide with each other.

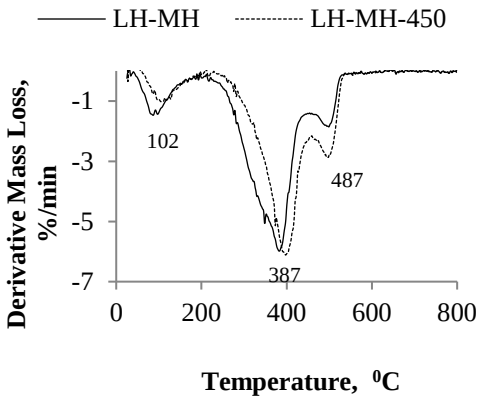

Figure 11. DTG curves.

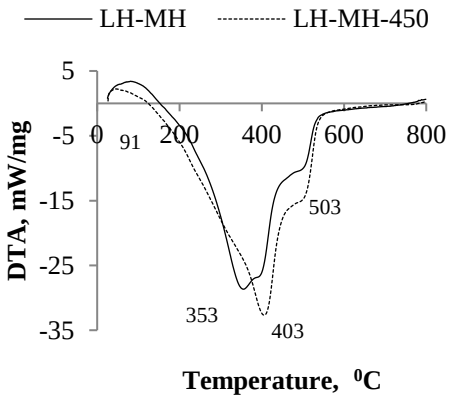

Figure 12. DTA curves.

However, it should be highlighted, that inorganic part (brucite) degradation shows as an endothermic peak, while organic part (lignin) degradation as exothermic one. Taking into account this confirmation, the peak of LH-MH (DTA curve, Fig.12) is smaller than the peak of LH-MH-450. LH-MH combine both organic and inorganic part when the temperature effects superimpose on one another. As a result emission of a heat due to degradation process decreased. The third peak associates with carbonate decomposition. This process occurs at the temperature around 500 ^{o}C.

According to Dufresne and Thomas (2013), addition of inorganic agents into the organic matrix ameliorates the thermostability of the product. In accordance with the present results (Fig.11), DTG curve shows the curve related to LH-MH-450 shifted by 10 ^{o}C to the right, which confirms that a coal from lignin is more thermally stable than the nanocomposite.

5.1.4. Investigation of the structure via XRD

X-ray patterns allow confirming the presence of crystalline structure in a material. As known, lignin is an amorphous polymer (Thomas and Visakh, 2012), that is why it cannot be observed by XRD. Thus, only the crystalline structure of the reinforcement agent (brucite) can be detected. Presence of the crystalline structure of $Mg(OH)_2$ in LH-MH can be confirmed by the peaks (Fig.13a) at $2\theta = 22.3^{o}$; 44.1^{o}; 61.5^{o} and 69.7^{o} (ICSD 98-020-3213). Zhu (2016) also reported about the brucite peaks at 22 and 60 degrees.

The disappearance of several peaks at the LH-MH-450 curve confirms the occurrence of extremely disordered structures, that are common for activated carbons, and are caused by the heat treating (Fu et al., 2011). However, presence of the crystalline structure of the reinforcer, transformed to the magnesium oxide due to the heat treating, is proved by the peaks (Fig.13b) at $2\theta = 51.7^{o}$ and 73.6^{o} (ICSD 98-015-9372). According to the observed results, presence of the reinforcer in the adsorption materials can be confirmed and thus the classification of the materials as composites proved.

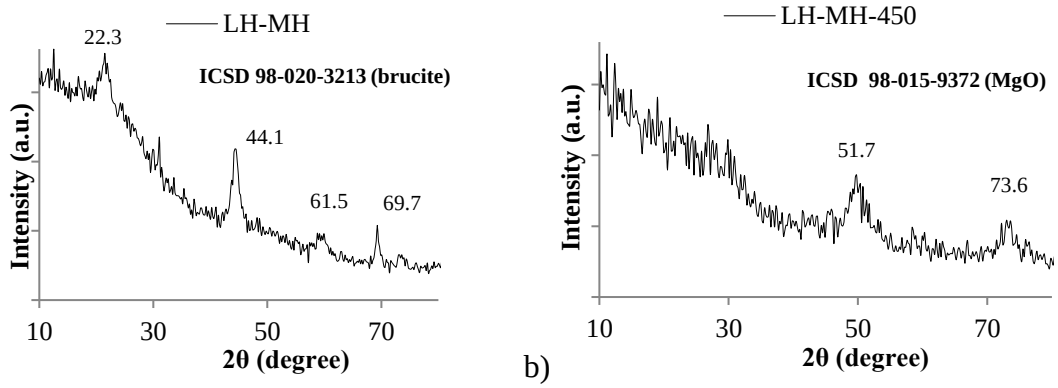

Figure13. X-ray diffraction patterns of (a) LH-MH and (b) LH-MH-450.

5.1.5. Morphology study via TEM

For examination of the morphological structure of the synthesized nanocomposites, TEM analysis was carried out. The best images of the nanocomposite structures were obtained in 25 k magnification (Fig. 14 a, b). It was found that particles of the reinforcing agent were integrated into an amorphous lignin structure in the form of rod-like nanocrystals. According to Ponomarev et al. (2017), the rod-like particles correspond to $Mg(OH)_2$ crystals. Brucite nanocrystals observed in LH-MH are 50-130 nm long and 15-20 nm wide. In that time, MgO nanoparticles in LH-MH-450, which came from brucite in the result of pyrolysis, have the length and width of 70-120 nm and 13-16 nm, respectively.

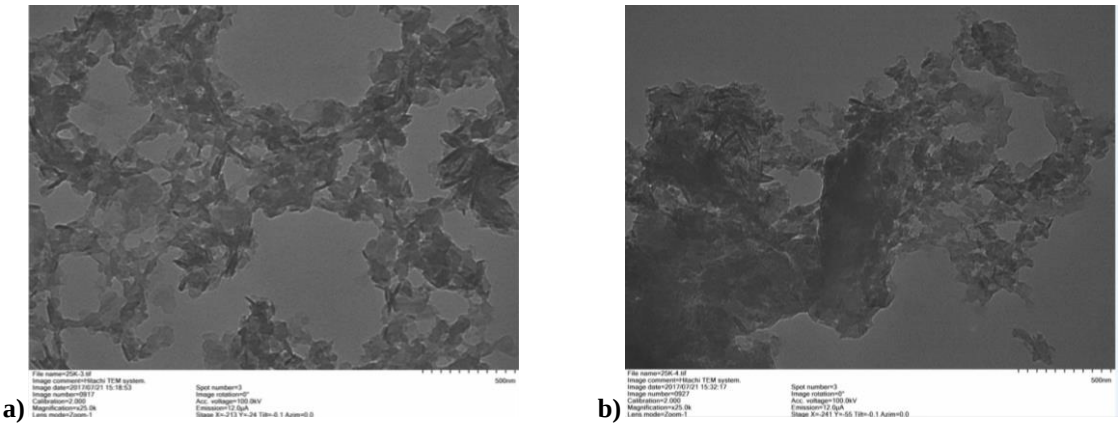

a) **b)**

Figure 14. TEM micrograph of LH-MH (a) and LH-MH-450 (b) nanocomposites.

5.2. Metal ions adsorption by LH-MH and LH-MH-450

5.2.1. Effect of adsorbent dose

The adsorption of Ni(II), Cd(II) and Pb(II) from 0.5 mmol/L solutions was studied as a function of dose of the adsorbents at neutral pH (Fig. 15-16). 20, 40, 60, 80, 100, 120, 140, and 160 mg of sample weights of the adsorbents were used. The increase of adsorption of Ni(II), Cd(II) and Pb(II) is noticed with increasing of adsorbent dose from 20 to 80 mg. Almost 100% removal of metal ions from the solutions was reached with 80 mg of adsorbents, which means that further increase of dose in the case of installed concentration is pointless. Thus, the optimal dose of adsorbent is 80 mg.

In comparison, LH-MH had better results than LH-MH-450. The uptake of metal ions onto LH-MH at the minimum adsorbent dose was almost 50%. In that time, the uptake at the minimum adsorbent dose for Cd(II) was 40%, for Ni(II) and Pb(II) – 20%. A little bit lower removal of Pb(II) by LH-MH-450 (coal form) can be explained by its rather high molecular weight and special aspects in interactions between the coal and lead ions.

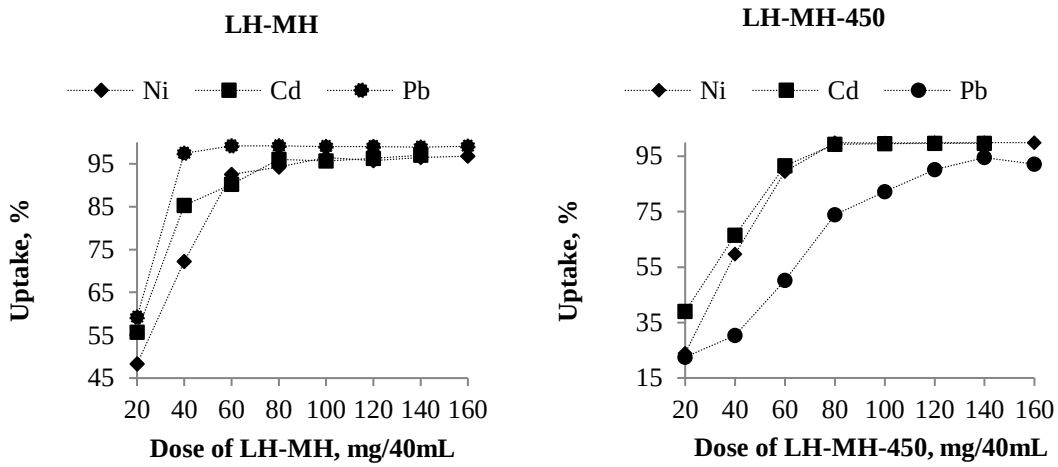

Figure 15. Effect of dose of LH-MH and LH-MH-450 for the removal of heavy metal ions. Initial concentrations for Ni(II), Cd(II) and Pb(II) - 0.5 mmol/L; pH: 5.5.

5.2.2. Effect of pH

Removal of Ni(II), Cd(II) and Pb(II) from 0.5 mmol/L solutions at different pH was studied. 80 mg of the adsorbent was used in 40 mL of solution. The pH range was chosen from 1 to 8. It can be seen that the adsorption efficiency of both LH-MH and LH-MH-450 increased as a function of pH. However, almost 100% removal of metal ions was observed starting from pH 3. The equilibrium capacity of Ni(II), and Cd(II) adsorption onto both LH-MH and LH-MH-450 in the pH range 3 – 8 was 15.5 mg/g and 28.9 mg/g, respectively. According to Figure 16, the optimal pH for Pb(II) removal onto both LH-MH and LH-MH-450 was between 3 and 6. After pH 6 the decrease of the adsorption was observed. However, maximum adsorption capacity for Pb(II) was 26.6 mg/g and 27.2 mg/g onto LH-MH and LH-MH-450, respectively.

The increase of adsorption at pH 3 can be explained by repulsive forces between metal cations and hydrogen ions, which concentration in acidic solutions is very high (Repo, 2011). As known, formation, and precipitation of insoluble metal hydroxides start at pH

higher than 7 (Iftekhar et al., 2017). That is why the adsorption in alkaline conditions would not occur only because of adsorbent properties, but also due to alkaline solution impact. As a result, it is possible to suggest that the optimal pH for obtained adsorption material was slightly acidic and neutral.

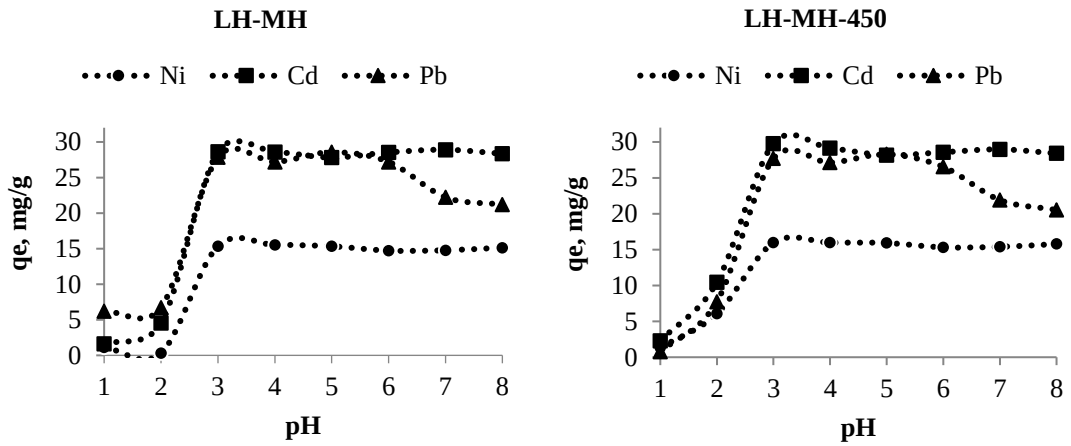

Figure 16. Removal of heavy metal ions by LH-MH and LH-MH-450 from the solutions at different pH. Dose: 2 g/L, initial concentrations: Ni(II) – 58.7 mg/L, Cd(II) – 112.4 mg/L, and Pb(II) - 207,2 mg/L.

5.2.3. pHzpc

To estimate the surface nature of synthesized nanocomposites pH_{zpc} plot was recorded (Fig.17). According with the obtained results, both materials have alkaline properties. pH_{zpc} is around 10 and 12 for LH-MH and LH-MH-450, respectively. This corresponds to the presence of hydroxyl groups, which are natural for raw material (lignin), and which promote precipitation of metal ions in the form of insoluble hydroxides. The results showed that the heat treatment encouraged the increase of alkalinity of the material. Thus, pH_{zpc} of LH-MH-450 was higher than that of LH-MH.

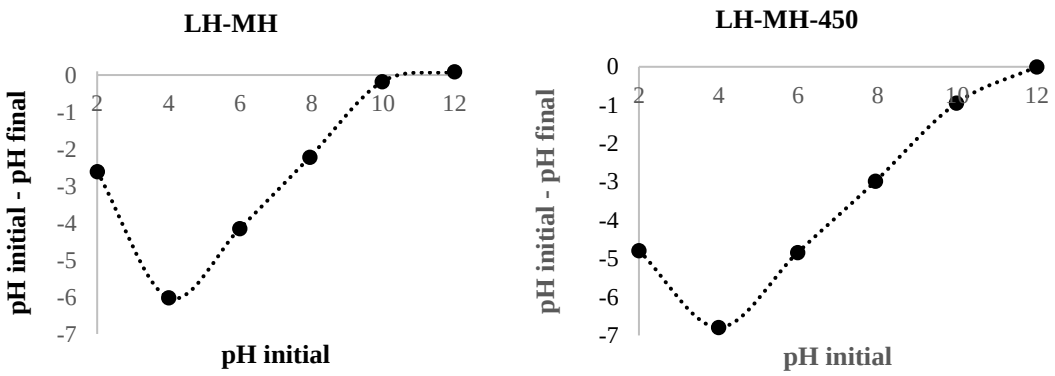

Figure 17. pH_{zpc} curves for LH-MH-and LH-MH-450.

5.2.4. Effect of temperature

As it can be observed from Figure 18, the increase of temperature did not effect on the adsorption efficiency. Thus, the increase of the temperature is not needed to improve the adsorption process. However, the effect of lower temperature should be investigated as well.

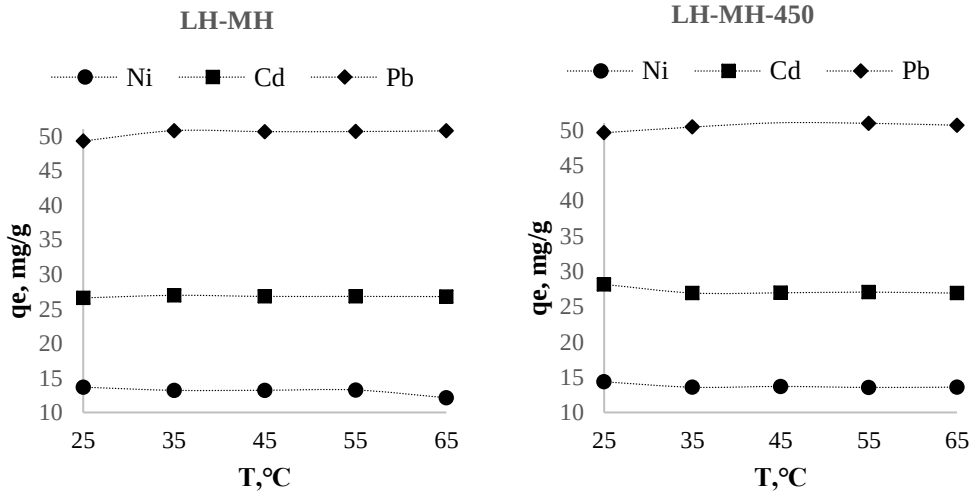

Figure 18. Effect of temperature for removal of heavy metal ions by LH-MH and LH-MH-450. Dose: 2 g/L, pH – 5.5, initial concentrations: Ni(II) – 58.7 mg/L, Cd(II) – 112.4 mg/L, and Pb(II) - 207,2 mg/L.

5.2.5. Effect of contact time

Both synthesized nanocomposites LH-MH and LH-MH-450 were investigated for the effect of contact time to estimate the desired time for saturation of the adsorbents. Comparison of obtained materials with commercially used activated carbon (GAC Norit EA 0.5-1,5) was carried out as well. The results of conducted tests are presented in Figures 19-20. Occupation of active sites by Ni(II), Cd(II) and Pb(II) onto LH-MH and LH-MH-450 happened in a similar way. However, there were some differences. Occupation of active sites by metal ions onto LH-MH happened very rapidly during the first 30 minutes. Then a slight decrease of the adsorption rate from 30 min to 3 h was noticed. However, during these 3 hours around 80% of each cation was removed. After 6 hours the system began to reach the equilibrium, and after 12 hours the system came into balance. The uptake of Ni(II), Cd(II) and Pb(II) onto LH-MH was 97; 98 and 99% respectively. Active occupation of active sites by metal ions onto LH-MH-450 was observed during the first 3 hours for Ni(II) and Pb(II) and during 4 h for Cd(II). Around 90% of substances were adsorbed at this time. After 6 hours the full saturation of adsorbent was reached. The uptake of cations by LH-MH-450 was 100% for Ni(II) and Cd(II) and 99% for Pb(II).

The uptake of Ni(II), Cd(II) and Pb(II) onto GAC was 45; 39 and 63% respectively. The diagram (Fig.20) is also showing more lengthened curves with longer time of slight adsorption rate from 1 to 4 hours. The rapid adsorption rate was observed during the first hour. The saturation of the adsorbent for Ni(II) was noticed after 6 h, for Cd(II) – after 12 h, and for Pb(II), according to Figure 23, equilibrium was not achieved even for 24 h.

It is possible to conclude, that 6 hours is optimal contact time for the metal adsorption onto LH-MH-450 and 12 h for LH-MH. However, further adsorption tests were carried out during 12 h to be sure of complete process termination. A preliminary short test of comparison between the synthesized nanocomposites and commercially used GAC confirmed high efficiency of novel materials and their potential to be applied in practice.

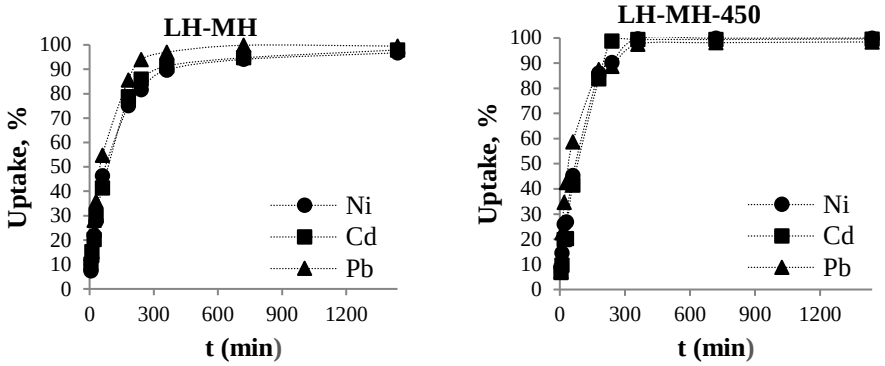

Figure 19. Effect of contact time for the removal of heavy metal ions by LH-MH and LH-MH-450. Dose: 2 g/L, pH – 5.5, initial concentrations: Ni(II) – 58.7 mg/L, Cd(II) – 112.4 mg/L, and Pb(II) - 207,2 mg/L.

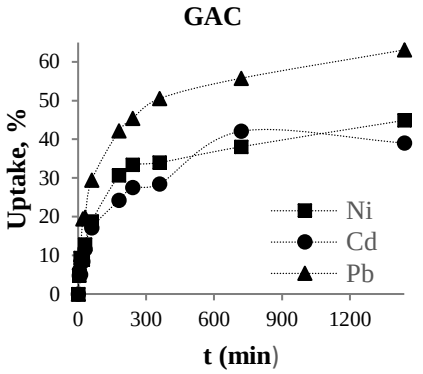

Figure 20. Effect of contact time for the removal of heavy metal ions by GAC. Dose: 2 g/L, pH – 5.5, initial concentrations: Ni(II) – 58.7 mg/L, Cd(II) – 112.4 mg/L, and Pb(II) - 207,2 mg/L.

5.2.6. Effect of initial metal concentration

Initial concentration study is one of the most important for estimation of adsorption efficiency. The results of variation of Ni(II), Cd(II) and Pb(II) as a function of initial concentration are presented in Figures 24 - 25 (paragraph 5.4.). For this study initial solutions of Ni(II), Cd(II) and Pb(II) were prepared in the range of 0.1-25 mmol/L. Because such a big concentrations are not detectable for analysis equipment (ICP-OES), the tested solutions were dissolved by DI water. It introduced some errors in the experiment. That is why the curves of the effect of initial concentration are rather fluctuated. However, it was possible to define that the maximum adsorption capacities of Ni(II), Cd(II) and Pb(II) adsorption onto LH-MH were 64; 106 and 272 mg/g, and onto LH-MH-450, 43; 91 and 128 mg/g respectively.

Obtained results of the adsorption capacities of the synthesized nanocomposites can be recognized rather high. For example, Berrima et al. (2016) reported about the following

adsorption capacities for the lignin-based charcoal: 83.9 mg/g for Ni(II), 72.9 mg/g for Cd(II) and 43.2 mg/g for Pb(II). Thus, it can be seen that LH-MH-450 was more efficient in the case of cadmium and lead removal. Celik and Dermirbas (2005) reported about Cd(II) and Pb(II) adsorption by modified lignin as 7.7 mg/g and 17.5 mg/g, respectively. Li et al. (2015) also reported a high Pb(II) adsorption capacity by the surface functionalized porous lignin that was 188 mg/g. It can be concluded that LH-MH – lignin-based nanocomposite showed a strong advantage over the modified lignin products and comparable results with surface functionalized lignin-based materials.

5.2.7. Influence of competing ions

In a multicomponent system, cations can be substituted by other ones because of similar ionic radius (Iftekhar et al., 2017). This fact possibly effects on the adsorption efficiency. For this reason, removal of Ni(II), Cd(II) and Pb(II) from their mixed solution and in the presence of competitive ions was checked. The results are presented in Tables 3 and 4.

Table 3. Adsorption efficiency for Ni(II), Cd(II) and Pb(II) in multicomponent system by LH-MH and LH-MH-450

	Ni	Cd	Pb
$C_{initial}$, mg/L	32	59	116
C_{final} (LH-MH)	2	4	0.3
Uptake, %	92	92	100
q_e, mg/g	15	27	58
C_{final} (LH-MH-450)	0.01	1.02	2.6
Uptake, %	100	98	98
q_e, mg/g	16	29	57

The obtained results showed that the adsorption efficiency for Ni(II), Cd(II) and Pb(II) from multicomponent solution was rather high in comparison with the previous results. 15 mg/g of Ni(II), 27 mg/g of Cd(II) and 58 mg/g of Pb(II) was adsorbed by the LH-MH from the multicomponent solution and 16, 29 and 57 mg/g of the listed ions were removed by the LH-MH-450. For example, average adsorption capacities of Ni(II), Cd(II) and Pb(II) from the monocomponent solutions onto LH-MH were 14; 27,5 and

49 mg/g; and 14; 28 and 49, 5 mg/g – onto LH-MH-450. Moreover, it can be seen that the adsorption capacity in the case of lead ion increased.

Table 4. Adsorption efficiency for Ni(II), Cd(II) and Pb(II) in multicomponent system with presence of competitive cations

	Ni	Cd	Pb	K	Na	Mg
$C_{initial}$, mg/L	31.1	57.6	115.8	21.9	13.1	13.1
C_{final} (LH-MH)	5.4	10	0.11	22.7	13.8	57.5
Uptake, %	83	83	100			
q_e, mg/g	13	24	58			
C_{final} (LH-MH450)	0.7	5.9	1.72	22.6	13.9	56.6
Uptake, %	98	90	99			
q_e, mg/g	15	26	57			

Presence of competitive ions does not have a strong effect on the removal of ions of interest as well. The adsorbed amount of the ions of interest did not much change. They were 13; 24 and 58 mg/g for Ni(II), Cd(II) and Pb(II) onto LH-MH, respectively; and 15; 26 and 57 mg/g for Ni(II), Cd(II) and Pb(II) onto LH-MH-450, respectively. It should be mentioned that competitive ions as K, Na and Mg were not removed by the tested adsorbents. This is due to the fact that ions of higher valence have a greater ability to be attracted by the surface of an adsorbent. Thus, all active sites of nanocomposites were occupied by divalent ions previously. Moreover, the increase of Mg(II) concentration in around 4 times was observed. It can be explained by the presence of Mg(II) in the form of the reinforcement agent in the nanocomposite, and its migration into the solution.

5.3. Modeling adsorption kinetics

The kinetics of Ni(II), Cd(II) and Pb(II) adsorption on synthesized nanocomposites was investigated using the pseudo-first and pseudo-second order kinetics models. Both linear and non-linear forms of the models were analyzed. They are illustrated in Figures 21-23. The unknown parameters of models were found by means of Solver MS Excel. Table 5 summarizes the values of kinetics parameters for both LH-MH and LH-MH-450.

Ho et al. (2000) reported that the non-linear forms of kinetic models are more suitable for the estimation of adsorption process because as the result of linearization of the original equations (eq. 5; 8) their structure change and adsorption parameters are determined with errors. That is why the non-linear models should be used firstly to obtain real values of the parameters.

Table 5. Kinetics parameters of non-linear and linear Pseudo First Order (PS1) and Pseudo Second Order (PS2) models for Ni(II), Cd(II) and Pb(II) adsorption onto LH-MH and LH-MH-450

Adsorbent	Element	$q_{e.exp}$ (mg/g)	PS1non-linear model			PS2non-linear model		
			$q_{e.cal}$ (mg/g)	k_1 (min^{-1})	R^2	$q_{e.cal}$ (mg/g)	k_2 (g/mg min)	R^2
LH-MH	Ni(II)	14.01	13.47	0.011	0.94	15.22	0.0009	0,98
	Cd(II)	27.48	28.41	0.011	0.94	31.85	0.0004	0.88
	Pb(II)	49.28	48.22	0.14	0.93	53.86	0.0003	0.96
LH-MH-450	Ni(II)	14.34	14.28	0.011	0.94	16.05	0.0009	0.98
	Cd(II)	28.14	28.98	0.010	0.94	32.94	0.0004	0.98
	Pb(II)	48.80	4.86	0.006	0.93	58.02	0.0001	0.97
			PS1linear model			PS2linear model		
LH-MH	Ni(II)	14.01	11.22	0.006	0.98	14.75	0.0010	0.99
	Cd(II)	27.48	8.71	0.003	0.36	28.81	0.0006	0.99
	Pb(II)	49.28	19.78	0.003	0.68	54.95	0.0003	0.99
LH-MH-450	Ni(II)	14.34	6.03	0.003	0.60	14.99	0.0012	0.99
	Cd(II)	28.14	11.22	0.004	0.68	30.49	0.0004	0.99
	Pb(II)	48.80	39.81	0.004	0.83	62.50	0.00006	0.87

The non-linear forms of both PS1 and PS2 show a good fitting with the experimental data (appendices IV). However, the correlation coefficients (R^2) were a little bit higher for PS2 than for PS1. This trend was observed for both tested materials and in the case of three metal ions of interest. There is only one exception with adsorption of Cd(II) by LH-MH for PS2 for which R^2 was only 88% instead of 94% and 98% obtained from the other calculations. The linear form of PS2 also demonstrated an excellent fitting with the experimental data. For all conducted tests, except Pb(II) on LH-MH-450, R^2 was 99%. In that time, fitting of PS1 linear model showed very poor results with the low correlation coefficients. Plazinski et al. (2013) also reported that the pseudo second model is more suitable in the case of solid/solution systems and gives a good correlation with the bivalent ions.

It also should be mentioned, that the adsorption rates k_1 and k_2 were higher in the case of nickel. It means that Ni(II) is adsorbed faster onto the adsorbent. It could be connected with its relatively small molecular mass in comparison with cadmium and lead ions.

Nevertheless, based on the results, the experimental data are better simulated by PS2 model. Pseudo-second order model assumes the surface reaction as a governing force of the adsorption kinetics (Repo, 2011). In other words, this model corresponds to the chemisorption as adsorption phenomena, which includes for example ion exchange and chelating mechanisms (Berrima et al., 2016).

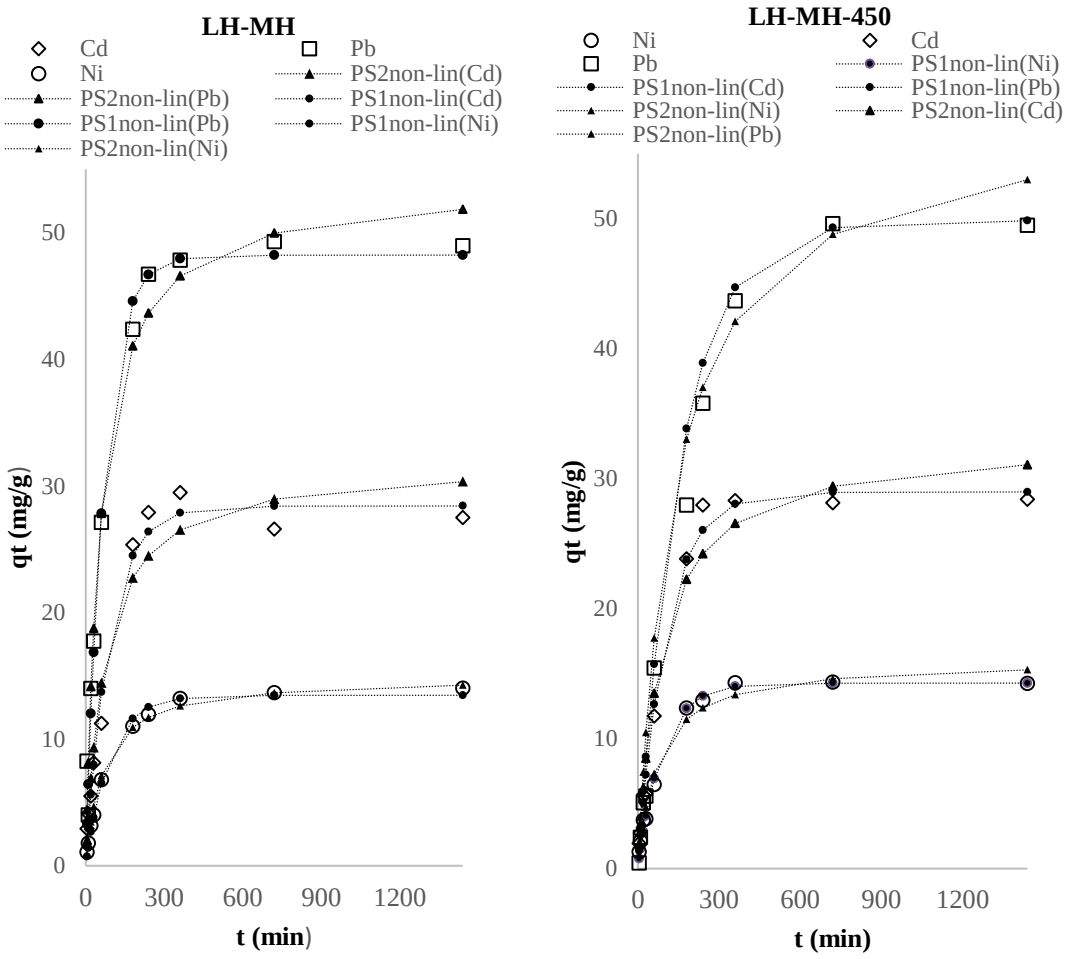

Figure 21. Plot of pseudo-first order (PS1) and pseudo-second order (PS2) non-linear models for adsorption of Ni(II), Cd(II) and Pb(II) onto LH-MH and LH-MH-450.

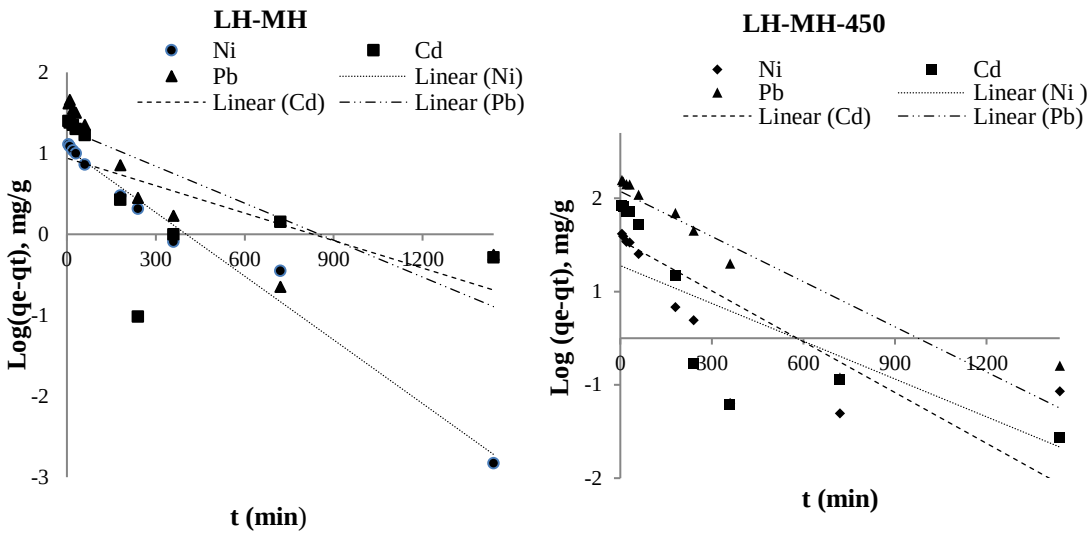

Figure 22. Plot of pseudo-first order linear model for adsorption of Ni(II), Cd(II) and Pb(II) onto LH-MH and LH-MH-450.

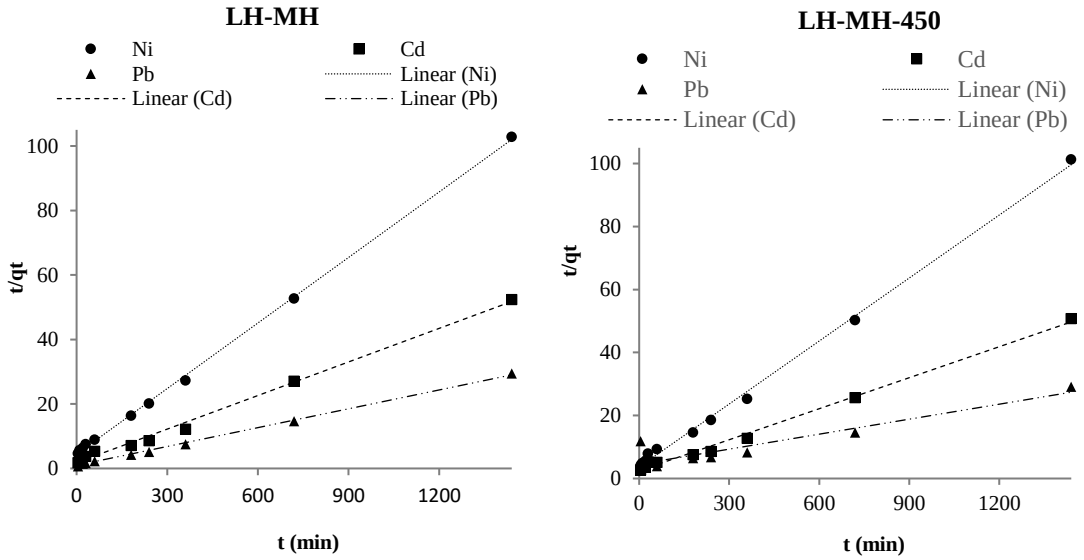

Figure 23. Plot of pseudo-second order linear model for adsorption of Ni(II), Cd(II) and Pb(II) onto LH-MH and LH-MH-450.

5.4. Modeling adsorption isotherms

Modeling of the adsorption isotherms is one of the important stages of determination of adsorption efficiency. They allow describing the interactions between the adsorbate and adsorbent and estimating the maximum adsorption capacity. Adsorption isotherms modeling was carried out on the base of initial concentrations data. The xperimental data was analyzed by Langmuir and Freundlich isotherm models (Fig. 24 – 25).

Parameters corresponding to the isotherm models are listed in Table 6. Unknown parameters were calculated with Solver MS Excel.

As can be seen from Figures 24 – 25, the isotherm plots correspond to L-type isotherm according to Giles' classification. Nevertheless, plots of Langmuir isotherms have a strict plateau in the case of Ni(II), Cd(II) and Pb(II) adsorption by both materials suggesting limited adsorption capacity of the adsorbents. Freundlich isotherms of all the tests have not a strict plateau meaning that the maximum adsorption capacity was not achieved.

According to Table 6, the high correlation coefficient (R^2) confirms well-fitting of both Langmuir and Freundlich models for Ni(II), Cd(II) and Pb(II) adsorption onto LH-MH. Taking into account that Langmuir and Freundlich models correspond to opposite characteristics of adsorbent (monolayer adsorption for Langmuir model, and multilayer adsorption for Freundlich model) and also the opposite behavior of the isotherms, it is impossible to provide any firm conclusions. Nevertheless, some assumptions can be done. According to Langmuir's suggestions about the monolayer adsorption, the adsorption onto LH-MH occurs due to natural functional groups of lignin and presence of $Mg(OH)_2$. The adsorption proceeds because of these conditions corresponds to chemisorption. LH-MH is also a material with a high surface area that is why it can accumulate substances by its pores enabling multilayer adsorption. However, Langmuir and Freundlich models are the simplest ones and cannot provide the accurate information about the system.

In the case of the metal ions adsorption by LH-MH-450, Freundlich isotherm has a better correlation with the experimental data (Table 6). This indicates the heterogeneous surface of the adsorbent (Repo, 2011) and multilayer adsorption. After the heat treatment, nanocomposite LH-MH-450 lost some functional groups but the pore sizes increased. That is why multilayer adsorption can be observed for this material.

It should be mentioned that variations in K_L values confirm different adsorption energies between the adsorbent and the metal ions and correlate with their adsorption rate (Hokkanen et al., 2014). According to the obtained results in Tables 6 and 5, Pb(II) had the biggest adsorption rate onto LH-MH, and Cd(II) – onto LH-MH-450.

Table 6. Isotherm constants for Ni(II), Cd(II) and Pb(II) adsorption by LH-MH and LH-MH-450

Adsorbent	Element	$q_{e.exp}$ (mg/g)	Langmuir			Freundlich		
			q_m (mg/g)	K_L (L/mg)	R_L^2	K_F (L/g)	n	R_F^2
LH-MH	Ni(II)	64	48.12	0.28	0.96	16.50	4.14	0.94
	Cd(II)	106	103.78	0.75	0.89	44.50	6.13	0.97
	Pb(II)	272	192.55	0.99	0.96	55.24	4.20	0.96
LH-MH-450	Ni(II)	43	46.66	0.22	0.59	23.46	7.57	0.98
	Cd(II)	91	92.25	0.81	0.65	49.90	9.31	0.99
	Pb(II)	128	127.44	0.25	0.94	41.91	4.55	0.94

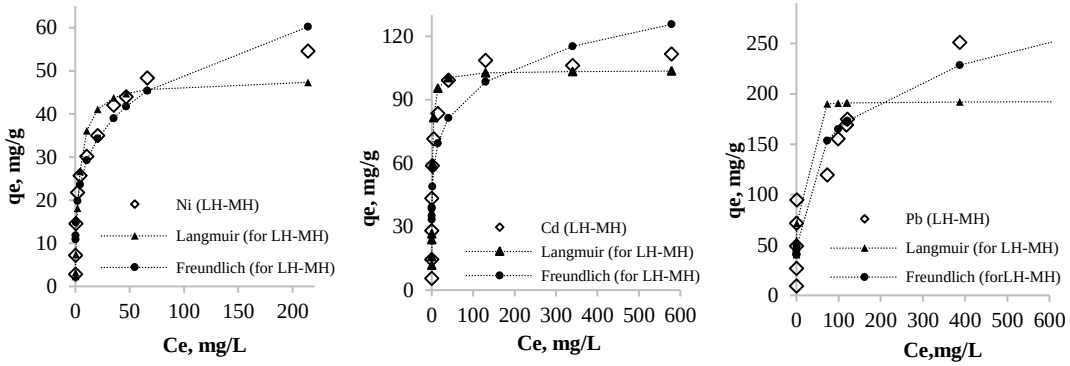

Figure 24. Experimental initial concentration data of Ni(II), Cd(II) and Pb(II) adsorption by LH-MH and comparison of Langmuir and Freundlich isotherm models.

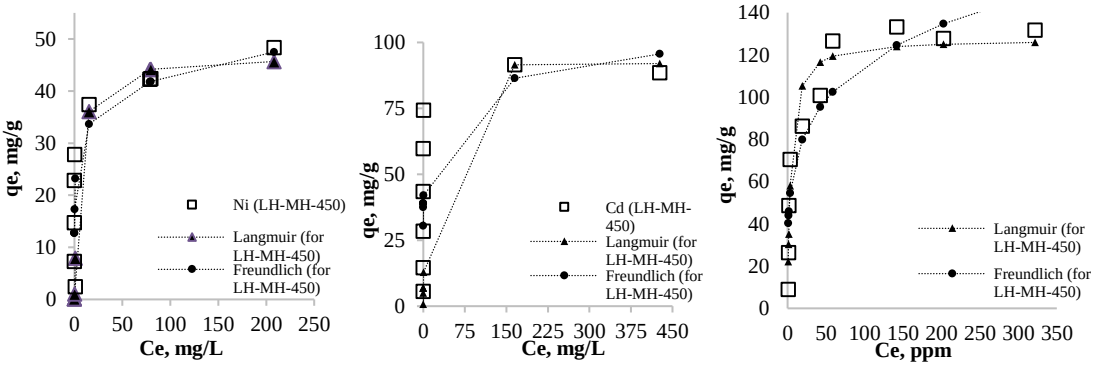

Figure 25. Experimental initial concentration data of Ni(II), Cd(II) and Pb(II) adsorption by LH-MH-450 and comparison of Langmuir and Freundlich isotherm models.

5.5. Regeneration study

Regeneration study was carried out to investigate the reusability of the synthesized materials. Desorption of metal ions from the surface of the adsorbents was conducted

by 0.1 M HNO_3. Samples of the adsorbents after the desorption cycle were studied via FTIR. The obtained IR-spectra show, that such a concentration of HNO_3 totally dissolves brucite added to the biopolymer structure. Therefore, the further desorption tests should be done with a lower concentration of the acid. IR-spectra before and after desorption are presented in Figure 26.

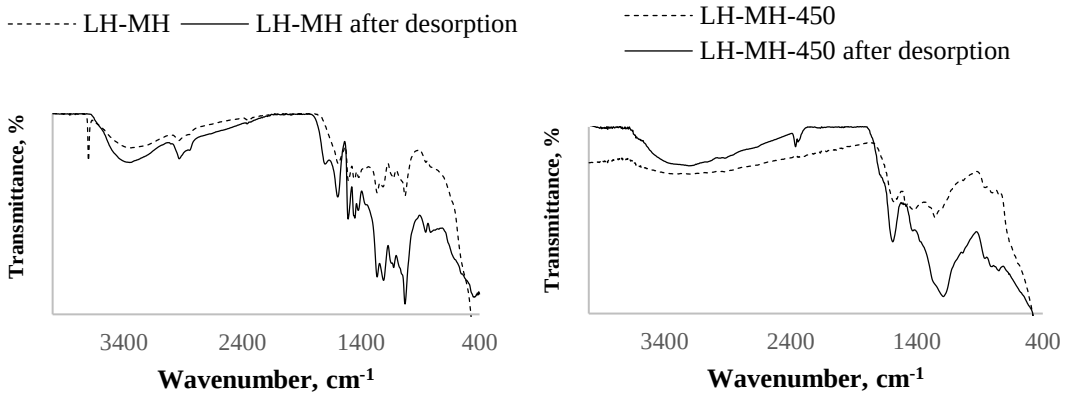

Figure 26. FTIR spectra of LH-MH and LH-MH-450 before and after adsorption.

5.6. Adsorption mechanism

The adsorption of heavy metal ions by LH-MH and LH-MH-450 can occur due to several mechanisms. Initially, the adsorption materials have the alkaline environment that is confirmed by pH_{zpc} plot. Therefore, due to the alkaline environment, metal ions interact with the surface OH groups of the adsorbents and precipitate on their surface. In the case of LH-MH, it is possible to suggest the same adsorption mechanism (chelation) due to OH groups that including into the reinforcement $Mg(OH)_2$.OH groups bind metal ions and promote their precipitation on the adsorbent surface. In terms of LH-MH-450, where $Mg(OH)_2$ was transformed into MgO, the ion-exchange mechanism is more believable. The exchange of Mg ions by heavy metal ions was confirmed via the test in presence of competitive ions, where the Mg concentration in the solution increased after the adsorption.

6 CONCLUSION AND FURTHER RESEARCH

In conclusion, it should be highlighted that novel lignin-based nanocomposite adsorption materials were produced. BET analysis confirmed that the materials include mesopores and have the highly developed specific surface area – 32.7 m^2/g and 20.6 m^2/g for LH-MH and LH-MH-450, respectively. Identification of the functional groups, typical for lignin, and new active sites, formatted because of reinforcement agent, were confirmed by FTIR. TEM micrographs and XRD patterns showed the affiliation of materials with nanocomposites. The sizes of nanoparticles presented in the material structures were proved as 50-130 nm long and 15-20 nm wide for LH-MH, and 70-120 nm long and 13-16 nm wide for LH-MH-450. Thermal stability of the synthesized materials was investigated based on the TGA and DTA. It was confirmed that the material degradation takes place at the temperature around 400 ^oC.

Numerous adsorption tests were carried out for investigating sorption properties of the synthesized materials. The optimal adsorbent dose was determined for the adsorption of Ni(II), Cd(II) and Pb(II) in 0.5 mmol/L solutions. The optimal dose was 80 mg for 40 mL of solution. Adsorption tests in different pH showed that the optimal pH range was slightly acidic and neutral. The pH_{zpc} study confirmed the alkaline environment for both LH-MH and LH-MH-450. It was also observed that temperature had not any significant impact on the adsorption process. Due to kinetics tests, the equilibrium contact time was determined as 6 and 12 hours for LH-MH and LH-MH-450 respectively. These tests also showed the advantages of the adsorption rate and sorption capacity between the tested nanocomposites and commercially used GAC. The adsorption capacities for Ni(II), Cd(II) and Pb(II) removal onto LH-MH were found to be 64; 106 and 272 mg/g respectively, and 43; 91 and 128 mg/g respectively onto LH-MH-450. Adsorption of metal ions of interest from the multicomponent solution and in the presence of competing ions confirmed the high efficiency of proposed materials in that case as well. Experimental kinetics data has the best fitting with the pseudo-second order model (non-linear). The Freundlich isotherm model fitted with the experimental data of the adsorption onto LH-MH-450. Both Langmuir and Freundlich isotherm models had a good fitting with the experimental adsorption data for LH-MH.

According to the conducted research, synthesized nanocomposites confirmed their potential to be used in the adsorption process. Obtained granulated materials are rather mechanically stable, simple and inexpensive in production, and quite efficient in the water purification process for Ni(II), Cd(II) and Pb(II) removal. Due to the biopolymer matrix synthesized nanocomposites are biodegradable, biocompatible, and renewable. These properties are extremely important for manufacturing of environmentally friendly chemical products.

The present topic is needed to be studied deeper. The further research should be aimed to the opportunity to use these materials for anion and organic matter removal. Additional adsorption and thermodynamic tests should be carried out to clarify the adsorption mechanism. The final step of this research can be conducting column tests with modeling of necessary equipment.

7 SUMMARY

The present research was focused on the development of a novel nanocomposite adsorption material. As the work was multipurpose and combined the material characterization via different analytical methods and the deep study of the adsorption properties, the full theoretical information about adsorption phenomena and description of the analytical methods were provided. The special focus was on biopolymers as a perspective matrix for the composite materials. For this reason, the features of the composites and especially nanocomposites were observed. Hydrolysis lignin was used as a basic biopolymer for this research. The information of its production, properties, and examples of the current use in the area of water treatment was presented as well.

The importance of water purification from Ni(II), Cd(II) and Pb(II) is rather high. Because they belong to the group of heavy metals. As known, heavy metal ions are hazardous for the environment and humanity. Due to the active anthropogenic activity, these substances come to the environment in the considerable amounts. Thus, they are needed to be removed and the adsorption process the most potential one.

Two lignin-based nanocomposites materials (LH-MH and LH-MH-450) were synthesized in the scopes of this research. Synthesis of novel materials included in reinforcing of the hydrolysis lignin by magnesium hydroxide via co-precipitation method. Magnesium hydroxide (or brucite) was chosen as a reinforcement agent due to its fibrous structure and high sorption properties in relation with heavy metal ions. After reinforcing stage, one part of the material was converted into a coal form by pyrolysis. It should be highlighted that the synthesized material was granulated and especially the granules were investigated via different adsorption tests.

Conducted TEM, XRD and FTIR analysis confirmed the presence of nanoparticles of brucite in the biopolymer matrix, also crystalline structure of reinforcing agent and functional groups typical for lignin were observed. Textural properties and particularly the specific surface area were examined via N_2 adsorption/desorption isotherms (BET method). The results of the analysis showed that the materials were mesoporous and had the highly developed specific surface area. Thermal stability was estimated by TGA and DTA.

Adsorption tests with synthesized nanocomposites were carried out with 0,5 mmol/L working solutions of Ni(II), Cd(II) and Pb(II) in the plastic tubes (50 mL). The adsorbent dose for all the tests was 80 mg. The adsorption properties were studied as the function of pH, temperature, contact time, and initial concentration. The kinetics and isotherm models were fitted to the obtained experimental data.

Results of conducted tests showed that a slightly acidic and neutral pH is suitable for the adsorption process by both LH-MH and LH-MH-450. Optimal contact time was 6 and 12 hours, which is less than the equilibrium time for the commercial granulated activated carbon (GAC). Moreover, novel materials showed a bigger adsorption capacity than GAC that confirms the perspectives of further use of the synthesized materials. The adsorption capacities for Ni(II), Cd(II) and Pb(II) removal onto LH-MH were found to be 64; 106 and 272 mg/g respectively, and 43; 91 and 128 mg/g respectively onto LH-MH-450. Adsorption of Ni(II), Cd(II) and Pb(II) from the multicomponent solution and in the presence of competitive ions as K, Na, and Mg(II) also showed high efficiency of the adsorbents. The presence of competitive ions and the multicomponent solution did not affect negatively the adsorption process. In the scopes of regeneration study 0.1 M HNO_3 dissolved brucite and thus could not be used to desorb the studies metals. This was confirmed by FTIR. That is why the regeneration study should be repeated with smaller acid concentrations.

Modeling of the kinetics models – the non-linear and linear Pseudo First Order (PS1) and Pseudo Second Order (PS2) models were conducted. Langmuir and Freundlich isotherm models were built as well. Unknown parameters of the models were found via ERRSQ method by means of MS Excel Solver Application. Experimental kinetics data has the best fitting with the pseudo-second order model (non-linear). The Freundlich isotherm model fits with the experimental data of the adsorption onto LH-MH-450. Both Langmuir and Freundlich isotherm models fitted well with the experimental adsorption data from LH-MH.

The conducted research confirmed the availability of the synthesized nanocomposites in the field of adsorption. However, the further research in the area of the determination of the adsorption mechanisms, potential to anions and organic matter removal, and column tests is highly recommended.

REFERENCES

Izotov, A. S. (2002) 'Mathematical Modeling of Metal Ion sorption on Brucite', *Journal of Mining Science*, 38(1), pp. 5–13.

Ajayan, P. M., Schadler, L. S. and Braun, P. V (2003) *Related Titles from Wiley-VCH Molecular Imprinting From Fundamentals to Applications Multilayer Thin Films Sequential Assembly of Nanocomposite Materials High Temperature Ceramic Matrix Composites Nanotechnology*. doi: 10.1002/3527602127.

Dufresne,A., Thomas, S. (2013) *Biopolymer Nanocomposites: Processing, Properties, and Applications*. Edited by Richard F. Grossman and Nwabunma Domasius. New Jersey: John Wiley & Sons, Inc.

Azizian, S., Haerifar, M. and Bashiri, H. (2009) 'Adsorption of methyl violet onto granular activated carbon: Equilibrium, kinetics and modeling', *Chemical Engineering Journal*, 146(1), pp. 36–41. doi: 10.1016/j.cej.2008.05.024.

Berrima, B., Maatar, W., Mortha, G., Boufi, S., Aloui, M. N. B. (2016) 'Adsorption of Heavy Metals on Charcoal From Lignin', 50, pp. 701–709.

Barakat, M. A. (2011) 'New trends in removing heavy metals from industrial wastewater', *Arabian Journal of Chemistry*. King Saud University, 4(4), pp. 361–377. doi: 10.1016/j.arabjc.2010.07.019.

Blanchard, G., Maunaye, M., Martin, G. (1984) 'REmoval of heavy matals from waters by means of natural zeolites', *Water Res.* 18 (12), 1501-1507.

Celik, A. and Demirbaş, A. (2005) 'Removal of heavy metal ions from aqueous solutions via adsorption onto modified lignin from pulping wastes', *Energy Sources*, 27(12), pp. 1167–1177. doi: 10.1080/00908310490479583.

Chen, S. *et al.* (2009) 'Studies on adsorption of phenol and 4-nitrophenol on MgAl-mixed oxide derived from MgAl-layered double hydroxide', *Separation and Purification Technology*, 67(2), pp. 194–200. doi: 10.1016/j.seppur.2009.03.016.

Christmann, K. (2011) 'Adsorption Practical relevance of adsorption processes Technical applications of adsorption concerns', (Lecture Series 2010/2011), pp. 1–39.

Christmann, K. (2012) 'Thermodynamics and Kinetics of Adsorption', *Institut für Chemie und Biochemie, Freie Universität Berlin*. Available at: http://w0.rz-berlin.mpg.de/imprs-cs/download/Vortrag_IMPRS_Schmoeckwitz_Mi_9-11_KChrist.pdf.

Chsrles H. Giles, D. S. (1974) 'A General Treatment and Classification of the Solute Adsorption Isotherm', 47(3).

Darder, M. *et al.* (2005) 'Bio-Nanocomposites Based on Layered Double Hydroxides', (3), pp. 1969–1977.

Duffus, J. H. (2002) '" HEAVY METALS "— A MEANINGLESS TERM ? (IUPAC Technical Report) (IUPAC Technical Report)', *Pure and applied chemistry*, 74(5), pp. 793–807.

Serc.carleton.edu. (2017). *X-ray plot*. [online] Available at: https://serc.carleton.edu/details/images/8418.html [Accessed 10 Oct. 2017].

Efimova, N. V *et al.* (2017) 'Sorption of heavy metals by natural biopolymers', *Adsorption Science & Technology*, 35(7–8), pp. 595–601. doi: 10.1177/0263617417703113.

Rouquerol, F., Rouquerol, J., Sing, K.S.W. (2014) *Adsorption by Powders and Porous Solids Principles, Methodology and Applications*. 2nd edn. Oxford: Elsevier Ltd.

Fedin, N., 2014. *Evaluation of the parameters of the porous structure and the specific surface area of nanoscale materials using an automatic gas adsorption analyzer TriStar*. (in Russian) [online] Available at: http://www.myshared.ru/slide/639242/ [Accessed 10 Oct. 2017].

Feldman, D. (2016) 'Lignin nanocomposites', *Journal of Macromolecular Science, Part A: Pure and Applied Chemistry*. Taylor & Francis, 53(6), pp. 382–387. doi: 10.1080/10601325.2016.1166006.

Fu, H. *et al.* (2011) 'Adsorption of Pharmaceuticals to Microporous Activated Carbon Treated with Potassium Hydroxide, Carbon Dioxide, and Steam', *Journal of Environment Quality*, 40(6), p. 1886. doi: 10.2134/jeq2011.0109.

Goudarzi, A., Lin, L.-T. and Ko, F. K. (2014) 'X-Ray Diffraction Analysis of Kraft Lignins and Lignin-Derived Carbon Nanofibers', *Journal of Nanotechnology in Engineering and Medicine*, 5(2), p. 21006. doi: 10.1115/1.4028300.

Hanke, L. (2001) 'Handbook of analytical methods for materials', *Materials Evaluation and Engineering, Inc*, pp. 1–50.

Hatakeyama, H. H. and T. (2009) 'Lignin Structure, Properties, and Applications', *Romanian Reports of Physics*, 54(3–4), pp. 349–359. doi: 10.1007/12 2009 12.

HITACHI, (2017). *Principle of ICP Optical Emission Spectrometry (ICP-OES)*. [online] Availiable at: http://www.hitachi-hightech.com/global/products/science/tech/ana/icp/descriptions/icp-oes.html [Accessed 3 October 2017].

Ho, Y. S., Ng, J. C. Y. and McKay, G. (2000) 'Kinetics of Pollutant Sorption By Biosorbents: Review', *Separation and Purification Methods*, 29(2), pp. 189–232. doi: 10.1081/SPM-100100009.

Hokkanen, S. *et al.* (2014) 'Adsorption of Ni2+, Cd2+, PO43- and NO3- from aqueous solutions by nanostructured microfibrillated cellulose modified with carbonated hydroxyapatite', *Chemical Engineering Journal*. Elsevier B.V., 252(3), pp. 64–74. doi:

10.1016/j.cej.2014.04.101.

Hou, X. and Jones, B. T. (2000) 'Inductively Coupled Plasma Optical Emission Spectrometry', *Encyclopedia of Analytical Chemistry*, pp. 9468–9485.

Iftekhar, S., Srivastava, V. and Sillanpää, M. (2017) 'Synthesis and application of LDH intercalated cellulose nanocomposite for separation of rare earth elements (REEs)', *Chemical Engineering Journal*, 309, pp. 130–139. doi: 10.1016/j.cej.2016.10.028.

Jawaid, M., Sapuan, M. and Alotman, O. (2017) *Green Biocomposities. Design and applications.* doi: 10.1007/978-3-319-49382-4.

Karmanov, A.P., Derkacheva, O. Y. (2012) 'Application of IR Fourier spectroscopy for the study of lignins of herbaceous plants', *Chemistry of plant raw material*, 1, pp. 61–70.

Kumar, M. and Chann, G. (2015) 'Nanocomposites in Wastewater Treatment', *Pan Stanford Publishing*, (April), p. 284.

Lagergren, S. (1898) 'About the theory of so-called adsorption of soluble substances', *K. Sven. Vetensk. Handl.* 24 (4), 1-39.

Langmuir, I. (1918) 'The adsorption of gases on plane surface of glass, mica and platinum', *J.Am. Chem. Soc.* 40 (9), 1361-1403.

Largitte, L. and Pasquier, R. (2016) 'A review of the kinetics adsorption models and their application to the adsorption of lead by an activated carbon', *Chemical Engineering Research and Design*. Institution of Chemical Engineers, 109, pp. 495–504. doi: 10.1016/j.cherd.2016.02.006.

Li, Z. *et al.* (2015) 'Surface-Functionalized Porous Lignin for Fast and Efficient Lead Removal from Aqueous Solution', *ACS Applied Materials and Interfaces*, 7(27), pp. 15000–15009. doi: 10.1021/acsami.5b03994.

Limousin, G. *et al.* (2007) 'Sorption isotherms: A review on physical bases, modeling and measurement', *Applied Geochemistry*, 22(2), pp. 249–275. doi: 10.1016/j.apgeochem.2006.09.010.

Lin, J. and Wang, L. (2009) 'Comparison between linear and non-linear forms of pseudo-first-order and pseudo-second-order adsorption kinetic models for the removal of methylene blue by activated carbon', *Frontiers of Environmental Science and Engineering in China*, 3(3), pp. 320–324. doi: 10.1007/s11783-009-0030-7.

Loganathan, P. *et al.* (2013) 'Defluoridation of drinking water using adsorption processes', *Journal of Hazardous Materials*. Elsevier B.V., 248–249(1), pp. 1–19. doi: 10.1016/j.jhazmat.2012.12.043.

Mainka, H. *et al.* (2015) 'Lignin - An alternative precursor for sustainable and cost-effective automotive carbon fiber', *Journal of Materials Research and Technology*. Korea Institute of Oriental Medicine, 4(3), pp. 283–296. doi: 10.1016/j.jmrt.2015.03.004.

Particle Analytical. *Introduction to BET*. [online] Available at: http://particle.dk/contact-us-analytical-lab oratory-2/ [Accessed 14 July 2017].

Pérez, N. A. *et al.* (2006) 'Use of biopolymers for the removal of heavy metals produced by the oil industry-A feasibility study', *Adsorption*, 12(4), pp. 279–286. doi: 10.1007/s10450-006-0504-x.

Plazinski, W., Dziuba, J. and Rudzinski, W. (2013) 'Modeling of sorption kinetics: The pseudo-second order equation and the sorbate intraparticle diffusivity', *Adsorption*, 19(5), pp. 1055–1064. doi: 10.1007/s10450-013-9529-0.

Po, H. *et al.* (2016) 'Hydrolysis Lignin as a Sorbent and Basis for Solid Composite Biofuel', pp. 501–530. doi: 10.4236/abb.2016.711046.

Ponomarev, N. *et al.* (2017) 'Green thermal-assisted synthesis and characterization of novel cellulose-Mg(OH)2 nanocomposite in PEG/NaOH solvent', *Carbohydrate Polymers*. Elsevier, 176(April), pp. 327–335. doi: 10.1016/j.carbpol.2017.08.101.

Ponomarev, N. (2017) '*Synthesis of Novel Cellulose Based Nanocomposites By Green Methods and Their Posible Use asAdsorbents*'. Master's Thesis. Lappeenranta University of Technology.

Popova, O. V., Serbinovskiy, M. Y. and Abramova, A. G. (2015) 'Development of technology for production and application of graphite from hydrolytic lignin', *European Journal of Wood and Wood Products*, 73(3), pp. 369–375. doi: 10.1007/s00107-015-0881-5.

Repo, E. (2011) *EDTA- and DTPA-Functionalized Silica Gel and Chitosan Adsorbents for the Removal of Heavy Metals from aqueous Solutions*. Doctoral dissertation. Lappeenranta University of Technology.

Rouquerolt, J. *et al.* (1994) 'Recommendations for the characterization of porous solids', *Pure & Appl. Chem.*, 66(8), pp. 1739–1758. doi: doi:10.1351/pac199466081739.

Sabu Thomas, P. M. Visakh, A. P. M. (2012) *Advances in Natural Polymers: Composites and Nanocomposites*. doi: 10.1007/978-3-642-14673-2.

Sampath, U. G. T. M. *et al.* (2016) 'Fabrication of porous materials from natural/synthetic biopolymers and their composites', *Materials*, 9(12), pp. 1–32. doi: 10.3390/ma9120991.

Sing, K. S. W. (1985) 'Reporting physisorption data for gas/solid systems with special reference to the determination of surface area and porosity (Recommendations 1984)', *Pure and Applied Chemistry*, 57(4), pp. 603–619. doi: 10.1351/pac198557040603.

Sharma, Y.C., Gupta, G.C., Prasad, G., Rupainwar, D.C, (1990) 'Use of wollastinite in the removal of Ni(II) from aques solutions',*Warter Air Soil Pollute*. 49 (1), 69-79.

Terzopoulou, Z., Kyzas, G. Z. and Bikiaris, D. N. (2015) 'Recent advances in nanocomposite materials of graphene derivatives with polysaccharides', *Materials*, 8(2), pp. 652–683. doi: 10.3390/ma8020652.

Tian, W. *et al.* (2017) 'Preparation, characterization and the adsorption characteristics of lignin/silica nanocomposites from cellulosic ethanol residue', *RSC Adv.* Royal Society of Chemistry, 7(65), pp. 41176–41181. doi: 10.1039/C7RA06322A.

MicroscopeMaster. (2017). *Transmission Electron Microscope (TEM) - Uses, Advantages and Disadvantages*. [online] Available at: http://www.microscopemaster.com/transmission-electron-microscope.html [Accessed 10 Oct. 2017].

Vainio, U. (2007) *Characterisation of cellulose- and lignin-based materials using X-ray scattering methods*. Available at: http://urn.fi/URN:ISBN:978-952-10-3256-1.

Xiao, S., Feng, J., Zhu, J., Wang, X., Yi, C., Su, S. (2013) 'Preparation and Characterization of Lignin-Layered Double Hydroxide/Styrene-Butadiene Rubber Composites Suo', *Applied Polymer Science*, pp. 13008–1312. doi: 10.1002/app.39311.

The KE Research Group. (2017). *The KE Research Group*. [online] Available at: http://www.keresearchgroup.com [Accessed 20 Sept. 2017].

Zhu, J. (2016) 'From Technical Lignin to Wood Lignin: An Evaluation of Two Approaches for Lignin Valorization', p. 73.

APPENDICES

Appendices I Effect of adsorbent amount

Table 7. ICP-OES measurements for different adsorbent sample weights

LH-MH				
Sample Name	m, mg	Element	Concentration, mg/L	Uptake,%
1 initial	0	Ni	26.95	0
20--1	20.12	Ni	13.94	48
40--1	39.93	Ni	7.49	72
60--1	59.66	Ni	2.02	93
80--1	80.42	Ni	1.55	94
100--1	99.89	Ni	0.95	96
120--1	119.72	Ni	1.14	96
140--1	140.08	Ni	0.94	97
160--1	159.98	Ni	0.87	97
2 initial	0	Cd	54.76	0
20--2	19.81	Cd	24.24	56
40--2	40	Cd	8.05	85
60--2	60.35	Cd	5.37	90
80--2	79.8	Cd	2.19	96
100--2	100.27	Cd	2.39	96
120--2	120.5	Cd	2.07	89
140--2	140.03	Cd	1.64	97
160--2	160.08	Cd	1.47	97
3 initial	0	Pb	105.31	0
20--3	19.55	Pb	42.95	59
40--3	40.21	Pb	2.72	97
60--3	60.29	Pb	0.87	99
80--3	80.11	Pb	0.85	99
100--3	99.9	Pb	1.01	99
120--3	120.4	Pb	1	99
140--3	140.46	Pb	1.22	99
160--3	159.6	Pb	0.95	99

LH-MH-450				
Sample Name	m, mg	Element	Concentration, mg/L	Uptake,%
1 initial	0	Ni	26.95	0
20--1--1	19.87	Ni	20.5	24
40--1--1	39.78	Ni	10.86	60
60--1--1	60.18	Ni	2.84	89
80--1--1	80.16	Ni	0.05	100
100--1--1	99.91	Ni	0.08	100
120--1--1	120.46	Ni	005	100
140--1--1	140.35	Ni	0,02	100
160--1--1	160.45	Ni	0.03	100
2 initial	0	Cd	54.76	0
20--2--1	20.39	Cd	33.4	39
40--2--1	40.14	Cd	18.32	67
60--2--1	59.72	Cd	4.6	92
80--2--1	79.62	Cd	0.4	99
100--2--1	99.66	Cd	0.26	100
120--2--1	120.18	Cd	0.21	100
140--2--1	139.65	Cd	0.2	100
160--2--1	160.47	Cd	0.26	100
3 initial	0	Pb	105.31	0
20--3--1	20.3	Pb	81.57	23
40--3--1	39.62	Pb	73.3	30
60--3--1	59.76	Pb	52.39	50
80--3--1	79.92	Pb	27.5	74
100--3--1	99.74	Pb	18.8	82
120--3--1	119.68	Pb	10.36	90
140--3--1	140.21	Pb	5.79	95
160--3--1	159.83	Pb	8.24	92

Appendices II Effect of pH

Table 8. ICP-OES measurements of removal heavy metal ions from solutions with different pH

LH-MH						
Name	Element	pH	m, mg	C_i, mg/L	C_e, mg/L	q_e, mg/g
1--1	Ni	1	79.73	30.2	27.96	1.12
2--1	Ni	2	79.53	32.59	26.96	0.32
3--1	Ni	3	80.30	32.11	1.32	15.34
4--1	Ni	4	79.54	31.95	1.06	15.,53
5--1	Ni	5	80.3	31.89	1.11	15.33
6--1	Ni	6	80.25	30.75	1.21	14.72
7--1	Ni	7	80.50	30.88	1.15	14.77
8--1	Ni	8	80.47	31,45	0.98	15.15
1--2	Cd	1	79.78	54.91	51.70	1.61
2--2	Cd	2	79.90	59.51	50.46	4.53
3--2	Cd	3	80.22	59.64	2.24	28.62
4--2	Cd	4	80.42	58.33	0.82	28.60
5--2	Cd	5	80.37	56.55	0.67	27.81
6--2	Cd	6	80.27	57.82	0.57	28.53
7--2	Cd	7	79.78	58.31	0.64	28.91
8--2	Cd	8	79.72	57.25	0.75	28.35
1--3	Pb	1	79.57	56.07	43.69	6.22
2--3	Pb	2	79.75	60.15	46.75	6.72
3--3	Pb	3	80.25	56.19	0.32	27.85
4--3	Pb	4	80.50	55.17	0.45	27.19
5--3	Pb	5	79.97	57.74	0.63	28.57
6--3	Pb	6	79.51	54.75	0.68	27.20
7--3	Pb	7	80.26	45.11	0.52	22.22
8--3	Pb	8	79.74	42.62	0.37	21.19

LH-MH-450						
Name	Element	pH	m, mg	C_i, mg/L	C_e, mg/L	q_e, mg/g
1--1--1	Ni	1	79.57	30.2	27.57	1.32
2--1--1	Ni	2	80.40	32.59	20.42	6.05
3--1--1	Ni	3	80.05	32.11	0.13	15.98
4--1--1	Ni	4	79.98	31.95	0.02	15.97
5--1--1	Ni	5	80.07	31.89	0.04	15.91
6--1--1	Ni	6	80.22	30.75	0.03	15.32
7--1--1	Ni	7	80.00	30.88	0.11	15.39
8--1--1	Ni	8	79.62	31.45	0.05	15.77
1--2--1	Cd	1	80.42	54.91	50.32	2.28
2--2--1	Cd	2	79.73	59.51	38.68	10.45
3--2--1	Cd	3	79.68	59.64	0.33	29.77
4--2--1	Cd	4	79.71	58.33	0.29	29.13
5--2--1	Cd	5	80.10	56.55	0.17	28.15
6--2--1	Cd	6	80.50	57.82	0.32	28.57
7--2--1	Cd	7	80.25	58.31	0.18	28.97
8--2--1	Cd	8	80.20	57.25	0.31	28.40
1--3--1	Pb	1	79.62	56.07	54.58	0.75
2--3--1	Pb	2	79.82	60.15	44.71	7.74
3--3--1	Pb	3	80.11	56.19	0.74	27.69
4--3--1	Pb	4	79.82	55.17	1.05	27.12
5--3--1	Pb	5	79.70	57.74	1.38	28.29
6--3--1	Pb	6	80.17	54.75	1.57	26.53
7--3--1	Pb	7	79.76	45.11	1.45	21.90
8--3--1	Pb	8	79.98	42.62	1.59	20.52

∗ C_i and C_e are the initial and the equilibrium concentrations (mg/L).

Appendices III Effect of temperature

Table 9. ICP-OES measurements of removal heavy metal ions from solutions in different temperature conditions

LH-MH					
Name	Element	m, mg	C_i, mg/L	C_e, mg/L	qe, mg/g
1	Ni		27.22	27.22	
298--1	Ni	79.68	28.93	1.72	13.66
308--1	Ni	80.09	27.22	0.79	13.20
318--1	Ni	80.09	27.22	0.77	13.21
328--1	Ni	80.32	27.22	0.61	1325
338--1	Ni	80.28	24.8	0.46	12.13
2	Cd		54.08	54.08	
298--2	Cd	80.02	56.13	2.97	26.57
308--2	Cd	79.62	54.08	0.44	26.95
318--2	Cd	79.86	54.08	0.59	2679
328--2	Cd	80.04	54.08	0.46	26.80
338--2	Cd	80.08	54.08	0.49	26.77
3	Pb		102.27	102.27	
298--3	Pb	79.91	98.98	0.54	49.28
308--3	Pb	80.08	102.27	0.62	50.77
318--3	Pb	80.33	102.27	0.59	50.63
328--3	Pb	80.25	102.27	0.66	50.65
338--3	Pb	80.1	1022.7	0.66	50.74

LH-MH-450					
Name	Element	m, mg	C_i, mg/L	C_e, mg/L	qe, mg/g
1	Ni		27.22	27.22	
298--1--1	Ni	79.65	28.59	0.03	14.34
308--1--1	Ni	80.18	27.22	0.01	1357
318--1--1	Ni	79.53	27.22	0.01	13.69
328--1--1	Ni	80.36	27.22	0.01	13.54
338--1--1	Ni	80.07	27.22	0.02	13.59
2	Cd		54.08	54.08	
298--2--1	Cd	80.21	56.79	0.36	28.14
308--2--1	Cd	80.27	54.08	0.05	26.92
318--2--1	Cd	80.17	54.08	0.08	26.94
328--2--1	Cd	79.83	54.08	0.1	27.05
338--2--1	Cd	80.2	54.08	0.15	26.90
3	Pb		102.27	102.27	
298--3--1	Pb	80.05	101.6	2.3	49.62
308--3--1	Pb	80.5	102.27	0.8	50.42
318--3--1	Pb	79.67	102.27	0.62	51.04
328--3--1	Pb	80.08	102.27	0.27	50.95
338--3--1	Pb	80.49	102.27	0.3	50.67

..

Appendices IV Effect of contact time and kinetics models

Table 10. ICP-OES measurements of removal heavy metal ions from solutions in different time onto LH-MH and parameters for kinetics models

Name	Time, min	Element	Ci, mg/L	Ct, mg/L	Ct, mmol/L	m, mg	V, mL	Uptake, %	q_t, mg/g	t/qt	qt PS2 non-lin	ERRSQ	qt PS1 non-lin	ERRSQ	qt PS1 lin Log (qe-qt)
5--1	5	Ni	28.93	26.79	0.46	79.8	40	7	1.07	4.67	0.91	0.03	0.72	0.12	1.13
10--1	10	Ni	28.93	25.37	0.43	80.13	40	12	1.78	5.63	1.97	0.04	1.41	0.14	1.10
20--1	20	Ni	28.93	22.57	0.38	80.46	40	22	3.16	6.33	3.48	0.10	2.67	0.24	1.05
30--1	30	Ni	28.93	20.91	0.36	80.11	40	28	4.00	7.49	4.68	0.46	3.80	0.04	1.02
60--1	60	Ni	29.35	15.76	0.27	80.17	40	46	6.78	8.85	7.12	0.12	6.53	0.06	0.89
180--1	180	Ni	29.35	7.32	0.12	80.11	40	75	11.00	16.36	10.93	0.00	11.63	0.39	0.54
240--1	240	Ni	29.35	5.38	0.09	80.21	40	82	11.95	20.08	11.71	0.06	12.52	0.32	0.41
360--1	360	Ni	29.35	3.02	0.05	79.76	40	90	13.20	27.26	12.61	0.35	13.22	0.00	0.11
720--1	720	Ni	28.93	1.72	0.03	79.68	40	94	13.66	52.71	13.67	0.00	13.46	0.04	-0.08
1440--1	1440	Ni	28.93	0.94	0.02	79.9	40	97	14.01	102.77	14.26	0.06	13.47	0.30	-0.31
Sum												1.22		1.65	
5--2	5	Cd	57.33	51.5	0.46	79.72	40	10	2.93	1.71	2.06	0.75	1.52	1.98	1.43
10--2--0	10	Cd	54.1	45.83	0.41	80.49	40	15	4.11	2.43	3.87	0.06	2.95	1.34	1.41
20--2--0	20	Cd	54.1	43.11	0.38	79.89	40	20	5.50	3.63	6.90	1.96	5.60	0.01	1.39
30--2--0	30	Cd	54.1	37.91	0.34	79.78	40	30	8.12	3.70	9.34	1.50	7.97	0.02	1.34
60--2--0	60	Cd	54.1	31.72	0.28	79.77	40	41	11.22	5.35	14.45	10.39	13.71	6.17	1.27
180--2	180	Cd	64.68	13.74	0.12	80.44	40	79	25.33	7.11	22.73	6.78	24.47	0.74	0.67
240--2	240	Cd	64.68	9.06	0.08	79.73	40	86	27.90	8.60	24.48	11.72	26.37	2.35	0.32
360--2	360	Cd	64.68	5.6	0.05	80.19	40	91	29.47	12.22	26.53	8.66	27.86	2.58	-0.28
12--2	720	Cd	56.13	2.97	0.03	80.02	40	95	26.57	27.09	28.95	5.64	28.40	3.34	0.53
24--2	1440	Cd	56.13	1.17	0.01	80	40	98	27.48	52.40	30.33	8.14	28.41	0.87	0.40
Sum												55.60		19.39	
5--3	5	Pb	113.84	97.38	0.47	79.75	40	14	8.26	0.61	4.40	14.87	3.34	24.21	1.62
10--3--0	10	Pb	98.98	90.95	0.44	80.07	40	14	4.01	2.49	8.14	17.01	6.44	5.90	1.66
20--3--0	20	Pb	98.98	71.09	0.34	79.74	40	28	13.99	1.43	14.14	0.02	12.02	3.88	1.56
30--3--0	30	Pb	98.98	63.42	0.31	80.17	40	36	17.74	1.69	18.74	1.00	16.86	0.79	1.51
60--3--0	60	Pb	98.98	44.72	0.22	80.09	40	55	27.10	2.21	27.81	0.50	27.82	0.52	1.36
180--3--0	180	Pb	98.98	14.25	0.07	80.03	40	86	42.35	4.25	41.04	1.71	44.57	4.94	0.88
240--3--0	240	Pb	98.98	5.97	0.03	79.68	40	94	46.69	5.14	43.64	9.33	46.68	0.00	0.52
360--3--0	360	Pb	98.98	2.98	0.01	80.32	40	97	47.81	7.53	46.58	1.50	47.95	0.02	0.34
12--3	720	Pb	98.98	0.54	0.00	79.91	40	100	49.28	14.61	49.96	0.46	48.22	1.11	-0.14
24--3	1440	Pb	98.98	0.49	0.00	80.49	40	99	48.95	29.42	51.83	8.34	48.22	0.52	0.02
Sum												54.74		41.88	

Appendices IV Effect of contact time and kinetics models

Table 11. ICP-OES measurements of removal heavy metal ions from solutions in different time onto LH-MH-450 and parameters for kinetics models

Name	Time, min	Element	Ci, mg/L	Ct, mg/L	Ct, mmol/L	m, mg	V, mL	Uptake, %	q_t, mg/g	t/q_t	qt PS2 non-lin	ERRSQ	qt PS1 non-lin	ERRSQ	qt PS1 lin Log (qe-qt)
5--1	5	Ni	28.59	26.05	0.49	79.59	40	9	1.28	3.92	1.05	0.05	0.77	0.26	1.12
10--2	10	Ni	28.59	24.42	0.49	79.9	40	15	2.09	4.79	1.97	0.01	1.50	0.35	1.09
20--1	20	Ni	28.59	21.14	0.49	80.25	40	26	3.71	5.39	3.50	0.04	2.83	0.77	1.03
30--1	30	Ni	28.59	20.90	0.49	80.3	40	27	3.83	7.83	4.74	0.82	4.03	0.04	1.03
60--1	60	Ni	28.59	15.62	0.49	80.19	40	45	6.47	9.27	7.32	0.72	6.93	0.21	0.90
180--1	180	Ni	28.59	3.98	0.49	79.76	40	86	12.34	14.58	11.48	0.74	12.33	0.00	0.33
240--1	240	Ni	28.59	2.79	0.49	79.73	40	90	12.94	18.54	12.36	0.34	13.27	0.11	0.19
360--1	360	Ni	28.59	0.08	0.49	79.76	40	100	14.30	25.18	13.39	0.83	14.01	0.08	-0.69
720--1	720	Ni	28.59	0.03	0.49	79.65	40	100	14.34	50.20	14.60	0.07	14.27	0.01	-0.80
1440--1	1440	Ni	28.59	0.02	0.49	80.31	40	100	14.23	101.20	15.29	1.13	14.27	0.00	-0.57
Sum												4.75		1.83	
5--2	5	Cd	56.79	52.95	0.51	80.19	40	7	1.92	2.61	1.80	0.01	1.35	0.32	1.43
10--2	10	Cd	56.79	51.26	0.51	80.49	40	10	2.75	3.64	3.41	0.44	2.64	0.01	1.42
20--2	20	Cd	56.79	45.47	0.51	80.18	40	20	5.65	3.54	6.18	0.28	5.04	0.37	1.37
30--2	30	Cd	56.79	45.25	0.51	80.5	40	20	5.73	5.23	8.47	7.51	7.22	2.20	1.37
60--2	60	Cd	56.79	33.24	0.51	80.27	40	41	11.74	5.11	13.48	3.05	12.64	0.81	1.24
180--2	180	Cd	56.79	9.20	0.51	79.93	40	84	23.82	7.56	22.24	2.48	23.78	0.00	0.71
240--2	240	Cd	56.79	0.71	0.51	80.2	40	99	27.97	8.58	24.21	14.16	26.05	3.69	0.01
360--2	360	Cd	56.79	0.35	0.51	79.76	40	99	28.30	12.72	26.55	3.06	28.05	0.07	-0.16
720--2	720	Cd	56.79	0.36	0.51	80.21	40	99	28.14	25.59	29.41	1.60	28.95	0.66	-0.07
1440--2	1440	Cd	56.79	0.24	0.51	79.61	40	100	28.41	50.68	31.07	7.08	28.98	0.32	-0.23
Sum												39.68		8.45	
5--3(1)	5	Pb	101.6	100.75	0.490347	80.41	40	7	0.42	11.83	2.06	2.66	1.55	1.27	1.70
10--3(1)	10	Pb	101.6	96.83	0.490347	79.66	40	23	2.40	4.18	3.97	2.48	3.05	0.43	1.68
20--3	20	Pb	101.6	91.45	0.490347	80.47	40	35	5.05	3.96	7.43	5.69	5.91	0.75	1.65
30--3	30	Pb	101.6	90.51	0.490347	79.59	40	43	5.57	5.38	10.48	24.03	8.60	9.14	1.65
60--3	60	Pb	101.6	70.67	0.490347	80.15	40	59	15.44	3.89	17.75	5.34	15.71	0.08	1.54
180--3	180	Pb	101.6	45.6	0.490347	80.12	40	87	27.96	6.44	33.03	25.77	33.84	34.63	1.34
240--3	240	Pb	101.6	30.06	0.490347	79.97	40	89	35.78	6.71	37.02	1.53	38.89	9.65	1.15
360--3	360	Pb	101.6	14.39	0.490347	79.88	40	97	43.67	8.24	42.10	2.47	44.71	1.09	0.80
720--3	720	Pb	101.6	2.3	0.490347	80.05	40	98	49.62	14.51	48.80	0.68	49.33	0.09	-0.42
1440--3	1440	Pb	101.6	2.33	0.490347	80.23	40	98	49.49	29.10	53.01	12.38	49.85	0.13	-0.29
Sum												83.03		57.24	

Appendices IV Effect of contact time

Table12. ICP-OES measurements of removal heavy metal ions from solutions in different time onto GAC (Norit EA 0.5-1.5) and parameters for kinetics models

Name	Time, min	Element	Ci, mg/L	Ct, mg/L	Uptake, %
5-1	5	Ni	32.31	0.550426	32.31
10-1	10	Ni	32.31	0.550426	30.77
20-1	20	Ni	32.31	0.550426	29.3
30-1	30	Ni	32.31	0.550426	29.44
60-1	60	Ni	32.31	0.550426	28.18
180-1	180	Ni	32.31	0.550426	26.24
240-1	240	Ni	32.31	0.550426	22.4
360-1	360	Ni	32.31	0.550426	21.52
720 -1	720	Ni	32.31	0.550426	21.33
1440 - 1	1440	Ni	32.31	0.550426	20.01
5-2	5	Cd	32.31	0.550426	17.81
10-2	10	Cd	59.61	0.530338	59.61
20-2	20	Cd	59.61	0.530338	56.76
30-2	30	Cd	59.61	0.530338	56.61
60-2	60	Cd	59.61	0.530338	54.58
180-2	180	Cd	59.61	0.530338	52.73
240-2	240	Cd	59.61	0.530338	49.43
360-2	360	Cd	59.61	0.530338	45.17
720 -2	720	Cd	59.61	0.530338	43.21
1440 - 2	1440	Cd	59.61	0.530338	42.64
5-3	5	Pb	59.61	0.530338	34.53
10-3	10	Pb	59.61	0.530338	36.34
20-3	20	Pb	109.58	0.528861	109.58
30-3	30	Pb	109.58	0.528861	100.72
60-3	60	Pb	109.58	0.528861	98,38
180-3	180	Pb	109.58	0.528861	88.3
240-3	240	Pb	109.58	0.528861	87.86
360-3	360	Pb	109.58	0.528861	77.32
720 -3	720	Pb	109.58	0.528861	63.4
1440 - 3	1440	Pb	109.58	0.528861	59.86

Appendices V Effect of initial concentrations and isotherm models

Table 13. ICP-OES measurements of removal heavy metal ions from solutions with different initial concentrations onto LH-MH and parameters for isotherm models

Name	Element	V, mL	m, mg	Ci, mg/L	Ce,mg/L	qe, mg/g	qe, Langmuir (mg/g)	ERRSQ	qm	48.12	qe, Freundlich(mg/g)	ERRSQ	K	16.50
0.1--1	Ni	40	79.96	5.8	0.18	2.81	2.32	0.241	KL	0.28	10.9	65.552	1/n	0.24
0.25--1	Ni	40	79.95	14.67	0.25	7.21	3.16	16.406			11.81	21.097	n	4.14
0.5--1	Ni	40	79.8	29.7	0.65	14.56	7.44	50.664			14.87	0.095		
0.75--1	Ni	40	80.25	45.81	2.14	21.77	18.09	13.508			19.82	3.780		
1--1	Ni	40	79.76	55.6	4.4	25.68	26.63	0.901			23.59	4.363		
1.25--1	Ni	40	79.96	70.9	10.7	30.12	36.13	36.160			29.23	0.784		
1.5--1	Ni	40	79.78	90.5	20.7	35.00	41.07	36.938			34.27	0.521		
2--1	Ni	40	79.57	119	35.4	42.03	43.73	2.917			39.01	9.083		
2.25--1	Ni	40	80.43	135.1	46.7	43.96	44.72	0.573			41.71	5.083		
2.5-1-10	Ni	40	79.74	162.6	66.2	48.35716	45.67	7.212			45.37	8.906		
5--1	Ni	40	80.34	323.9	214.2	54.61787	47.34	53.005			60.23	31.548		
Sum								218.525				150.813		
0,.--2	Cd	40	79.64	11.21	0.24	5.51	15.79	105.643	qm	103.78	35.25	884.701	K	44.50
0.25--2	Cd	40	80.48	29.26	0.17	14.46	11.70	7.594	KL	0.75	33.32	355.941	1/n	0.16
0.5--2	Cd	40	80.2	56.77	0.46	28.08	26.56	2.334			39.20	123.603	n	6.13
0.75--2	Cd	40	79.93	87.1	0.4	43.39	23.89	380.152			38.32	25.700		
1--2	Cd	40	79.84	119.2	1.8	58.82	59.54	0.518			48.98	96.810		
1.25--2	Cd	40	80.19	148.3	4.9	71.53	81.53	99.909			57.67	191.995		
15--2	Cd	40	80.45	183	15.2	83.43	95.39	142.939			69.38	197.530		
.--2	Cd	40	79.91	238.6	40.3	99.26	100.45	1.404			81.34	321.119		
3--2	Cd	40	80	347.2	129.9	108.65	102.72	35.133			98.46	103.819		
5--2	Cd	40	80.48	553.9	340.2	106.21	103.37	8.058			115.21	80.982		
7.5--2	Cd	40	79.9	802	579	111.64	103.54	65.582			125.66	196.468		
Sum								849.267				2578.667		
0.1--3	Pb	40	80.2	18.64	0.27	9.16	40.47	979.945	qm	192.55	40.43	977.574	K	55.24
0.25--3	Pb	40	80.4	53.83	0.28	26.64	41.64	224.970	KL	0.99	40.78	199.896	1/n	0.24
0.5--3	Pb	40	80	98.4	0.4	49.00	54.44	29.606			44.40	21.171	n	4.20
0.75--3	Pb	40	80.4	143.8	0.3	71.39	43.94	753.863			41.46	896.201		
1-3	Pb	40	80.39	190.7	0.6	94.59	71.55	530.914			48.90	2087.112		
1-5--3	Pb	40	80.17	312.2	72.7	119.50	189.90	4956.962			153.44	1151.993		
2--3	Pb	40	79.75	408.4	98.7	155.34	190.59	1243.091			165.04	94.110		
2.25--3	Pb	40	80	456.5	118.4	169.05	190.92	478.130			172.35	10.908		
3--3	Pb	40	80.12	471	121	174.74	190.95	262.866			173.25	2.221		
5--3	Pb	40	79.54	886	387	250.94	192.05	3468.509			228.57	500.560		
7.5--3	Pb	40	80.5	1347	799	272.30	192.31	6398.389			271.68	0.379		
Sum								19327.247				5942.125		

Appendices V Effect of initial concentrations and isotherm models

Table 14. ICP-OES measurements of removal heavy metal ions from solutions with different initial concentrations onto LH-MH-450 and parameters for isotherm models

Name	Element	m, mg	V, mL	Ci, mg/L	Ce,mg/L	qe, mg/g	qe, Langmuir (mg/g)	ERRSQ	qm	46.658	qe, Freundlich(mg/g)	ERRSQ	K	23.461
0,1--1--1	Ni	80.240	40	5.800	0.920	2.433	7.949	30.427	K_L	0.223	23.204	431.442	1/n	0.132
0,25--1--1	Ni	80.100	40	14.670	0.010	7.321	0.104	52.084			12.766	29.652	n	7.568
0,5--1--1	Ni	80.460	40	29.700	0.010	14.760	0.104	214.805			12.766	3.976		
0,75--1--1	Ni	80.110	40	45.810	0.010	22.869	0.104	518.229			12.766	102.058		
1--1--1	Ni	79.780	40	55.600	0.100	27.827	1.019	718.660			17.306	110.676		
1,5--1--1	Ni	80.340	40	90.500	15.300	37.441	36.090	1.825			33.643	14.424		
2.5-1-1-10		79.610	40	162.600	78.500	42.256	44.139	3.546			41.758	0.248		
2,75--1--1	Ni	80.150	40	164.500	79.500	42.420	44.169	3.057			41.828	0.351		
5--1--1	Ni	80.200	40	305.200	208.200	48.379	45.675	7.310			47.502	0.768		
Sum			40					1549.944				693.595		
0,1--2--1	Cd	80.120	40	11.210	0.070	5.562	4.964	0.357	qm	92.252	37.506	1020.435	K	49.904
0,25--2--1	Cd	80.500		29.260	0.010	14.534	0.743	190.185	K_L	0.812	30.433	252.759	1/n	0.107
0,5--2--1	Cd	80.000	40	56.770	0.100	28.335	6.931	458.113			38.970	113.113	n	9.311
0,75--2--1	Cd	80.000	40	87.100	0.100	43.500	6.931	1337.261			38.970	20.517		
1--2--1	Cd	79.740	40	119.200	0.100	59.744	6.931	2789.187			38.970	431.546		
1,25--2--1	Cd	79.720	40	148.300	0.200	74.310	12.894	3771.932			41.982	1045.090		
3--2--1	Cd	79.540	40	347.200	165.300	91.476	91.570	0.009			86.371	26.059		
5--2--1	Cd	80.500	40	605.000	427.000	88.447	91.986	12.527			95.639	51.716		
Sum			40					8559.571				2961.236		
0,1--3--1	Pb	80.500	40	18.640	0.830	8.850	22.108	175.790	qm	127.439	40.227	984.556	K	41.909
0,25--3--1	Pb	79.950	40	53.830	1.230	26.316	30.235	15.355	K_L	0.253	43.860	307.775	1/n	0.220
0,5--3--1	Pb	79.850	40	98.400	1.500	48.541	35.047	182.095			45.815	7.429	n	4.550
0,75--3--1	Pb	79.730	40	143.800	3.300	70.488	57.972	156.657			54.485	256.101		
1--3--1	Pb	79.700		190.700	18.800	86.274	105.292	361.692			79.866	41.055		
1,25--3--1	Pb	79.860	40	243.100	42.100	100.676	116.496	250.279			95.350	28.373		
1,5--3--1	Pb	80.240	40	312.200	58.400	126.520	119.357	51.318			102.461	578.858		
2--3--1	Pb	80.090	40	408.400	141.700	133.200	123.979	85.033			124.500	75.686		
2,25--3--1	Pb	79.610	40	456.500	202.400	127.672	124.997	7.160			134.649	48.677		
2,75--3--1	Pb	80.240	40	585.500	321.400	131.655	125.890	33.238			149.055	302.763		
Sum								1318.617				2631.272		